A Search for the Rare and Forbidden Decays $D^0 \to V\ell^+\ell^-$

A Dissertation

Presented for the

Doctor of Philosophy

Degree

The University of Mississippi

Eric M. Aitala

December 2003

Dedication

To Mom, Dad, and Sheryl.

"There is a difference between something being complicated and something being complex..."

Jon Hackett, *Decipher*

Acknowledgments

I would like to thank David Sanders, Romulus Godang, Don Summers, Lucien Cremaldi, Ali Rafatian, Jeff Appel, Steve Bracker, Ai Nguyen, Milind Purohit, Alan Schwartz, Jean Slaughter, Noel Stanton, Nick Witchey, Krish Gounder, Ray Stefanski, Robert Jedicke, Colin Gay, Larry Crum, and all the members of the Fermilab E791 collaboration. Also many thanks to the staffs of Fermilab and participating institutions. This research was supported by the Brazilian Conselho Nacional de Desenvolvimento Científico e Tecnológico, CONACyT (Mexico), the Israeli Academy of Sciences and Humanities, the U.S.-Israel Binational Science Foundation, the U.S. National Science Foundation and the U.S. Department of Energy.

Abstract

I report the results of a search for flavor-changing neutral current, lepton-flavor, and lepton-number violating decays of the 3 and 4-body decay modes of the D^0 (and its antiparticle) containing muons and electrons. Using data from Fermilab charm hadroproduction experiment E791, I examine modes with two leptons and either a ρ^0, $\overline{K}^{*0}$, or ϕ vector meson or a non-resonant $\pi\pi$, $K\pi$, or KK pair of pseudoscalar mesons. No evidence for any of these decays is found. Therefore, branching-fraction upper limits, typically at the 10^{-4} level, are presented at the 90% confidence level for the 27 decay modes examined. Of these searches, 18 are investigations of decays without previous published results; several others have significantly improved sensitivity over previous results.

Contents

List of Figures

List of Tables

Chapter 1

Introduction

The E791 Experiment [1, 2, 3] at Fermilab's Tagged Photon Lab (TPL) yielded a vast quantity (see Table 1.1) of high energy physics data. The experiment collected 200 000 fully reconstructed charmed hadron decays, the world's largest sample at the time it ran. This created the necessity for a means to analyze the data in a timely and efficient manner. To this end, large parallel processing computer farms were assembled at the Kansas State University, Fermilab, CBPF–Rio de Janeiro, and the University of Mississippi. A primary mission of the experiment is the search for rare and forbidden decays of charmed particles, such as the D meson. An earlier search focussed on rare decays of the charged D meson [4, 5] while this

analysis [6] will focus on three– and four–particle decays of the neutral D. See Table 1.2 for a description of the D^0 meson.

Table 1.1: Comparison of the size of raw data sets processed by Fermilab E791 with estimates from several $p\overline{p}$, e^-p, and e^+e^- collider experiments. D0 records digitized waveforms for its central detector which increases its data set size. The number of events recorded at LEP includes triggers such as Bhabhas as well as Z^0 triggers.

Experiment	Events Recorded Millions	Raw Data Recorded Terabytes	Recording Period
FNAL E791	20 000	50	7/91 - 1/92
FNAL CDF	95	10	10/85 - 12/95
FNAL D0	80	40	2/92 - 12/95
HERA H1	70	2.5	5/92 - 12/95
HERA ZEUS	50	5	5/92 - 12/95
LEP ALEPH	60	1.7	8/89 - 11/95
LEP DELPHI	∼30	∼5	8/89 - 11/95
LEP L3	83	3.4	8/89 - 11/95
LEP OPAL	102	1.5	8/89 - 11/95
CESR CLEO	600	5	10/79 - 12/95

An analysis into rare and forbidden decays is vital in probing the Standard Model (SM) and for searching for further new physics [7]. While

Table 1.2: D^0 Meson Statistics.

Physical Parameter	D^0
Mass	1.864 GeV
Quark Content	$c\bar{u}$
Lifetime	4.21 $\times 10^{-13}$ s
Primary Charged Decay	$K^-\pi^+$, $K^-\pi^+\pi^-\pi^+$

the SM can make many qualitative and quantitative predictions concerning particles such as decay modes and decay rates, there are areas in which its predictive ability fails. It cannot, for example, predict the number of families of quarks or leptons. It cannot account for the masses of the various particles, nor can it account for the number of fundamental forces. It is therefore necessary to examine unusual and forbidden areas within the Standard Model to search for new physics in order to extend its reach. Decays involving the more massive, lesser studied particles, such as charmed mesons, could result in the discovery of new particles or a new gauge boson, and thus a new fundamental force [8, 9].

In this analysis, twenty-seven decays modes of the D^0 charmed meson into resonant and non-resonant modes containing two leptons have been examined (see Table 1.3 for resonant and Table 1.4 for non-resonant). The

Table 1.3: D^0 Resonant Decays: FCNC – Flavor Changing Neutral Current and LFV – Lepton Flavor Violating.

Decay Modes	Decay Type
$D^0 \to \bar{K}^{*0}\mu^+\mu^-$	FCNC
$D^0 \to \bar{K}^{*0}e^+e^-$	FCNC
$D^0 \to \bar{K}^{*0}\mu^+e^-$	LFV
$D^0 \to \phi\mu^+\mu^-$	FCNC
$D^0 \to \phi e^+e^-$	FCNC
$D^0 \to \phi\mu^+e^-$	LFV
$D^0 \to \rho^0\mu^+\mu^-$	FCNC
$D^0 \to \rho^0 e^+e^-$	FCNC
$D^0 \to \rho^0\mu^+e^-$	LFV

resonant decay modes of interest are of the form $D^0 \to V\ell^+\ell^-$, where V is either a rho (ρ), an anti-kaon ($\bar{K}^{*0}$), or a phi (ϕ) vector meson. The non-resonant modes of interest are of the form $D^0 \to hh\ell\ell$, where h is either a pion (π) or kaon (K) pseudo-scalar meson. Charge conjugate decays are included implicitly.

A blind analysis method will be used to search for these rare decays – the region of interest in the data is 'boxed' out, or hidden from analysis. All cuts made on the data set are determined using the noise from the

Table 1.4: D^0 Non-Resonant Decays: FCNC – Flavor Changing Neutral Current, LFV – Lepton Flavor Violating, and LNV – Lepton Number Violating.

Decay Modes	Decay Type
$D^0 \to \pi^+\pi^-\mu^+\mu^-$	FCNC
$D^0 \to \pi^+\pi^-e^+e^-$	FCNC
$D^0 \to \pi^+\pi^-\mu^\pm e^\mp$	LFV
$D^0 \to \pi^-\pi^-\mu^+\mu^+$	LNV
$D^0 \to \pi^-\pi^-e^+e^+$	LNV
$D^0 \to \pi^-\pi^-\mu^+e^+$	LNV
$D^0 \to K^-\pi^+\mu^+\mu^-$	FCNC
$D^0 \to K^-\pi^+e^+e^-$	FCNC
$D^0 \to K^-\pi^+\mu^\pm e^\mp$	LFV
$D^0 \to K^-K^+\mu^+\mu^-$	FCNC
$D^0 \to K^-K^+e^+e^-$	FCNC
$D^0 \to K^-K^+\mu^\pm e^\mp$	LFV
$D^0 \to K^-\pi^-\mu^+\mu^+$	LNV
$D^0 \to K^-\pi^-e^+e^+$	LNV
$D^0 \to K^-\pi^-\mu^+e^+$	LNV
$D^0 \to K^-K^-\mu^+\mu^+$	LNV
$D^0 \to K^-K^-e^+e^+$	LNV
$D^0 \to K^-K^-\mu^+e^+$	LNV

unboxed data regions as background, while the 'signal' is created using a set of simulated Monte Carlo data. Cuts are established by varying a set of appropriate physical parameters and determining the values at which the highest signal to noise ratio is found.

Once 'unboxed' the branching ratio for each decay mode can be calculated using the Monte Carlo data, the normalization mode data, the signal data, and the background data.

Because we expect a small, or non-existent, signal size, using traditional methods for determining upper confidence levels is not appropriate. Therefore, a specialized method will be used to calculate the upper limit of each branching ratio and incorporate systematic errors.

Chapter 2

The Standard Model and Rare Decays of Charm Mesons

The Standard Model describes all experiments on matter and forces in the universe (except for gravity) and explains the hundreds of particles and their complex interactions in terms of fundamental particles and interactions. There are two types of fundamental particles within the model:

- Fundamental Matter Particles:
  - fermions - spin 1/2 particles - subject to the Pauli Exclusion Principle.

    * leptons (electron, muon, and tau, plus their associated neutrinos).
    * quarks (up, down, strange, charm, bottom, top).

- Force Carrier Particles:
  - bosons - integral spin particles.
  - each fundamental interaction (electromagnetic, weak, and strong) mediated by a force-carrier particle.
    * photons, $W^{\pm}$, Z^0, and gluons.

2.1 Flavor Changing Neutral Currents, Lepton Family Violating Decays, and Lepton Number Violating Decays

A search for flavor changing neutral current (FCNC), lepton family violating (LFV), or lepton number violating (LNV) decays is a primary method for probing physics outside the Standard Model. An FCNC decay is one where one flavor of quark decays into another via the emission of a neutral particle, hence the term 'neutral current'. The most sensitive, previous

FCNC studies have been upon particles containing strange quarks, which have charge minus one-third. The charm quark carries a charge of positive two-thirds. The possibility exists for differences in the FCNC rates between these two quarks [10].

A LFV decay (e.g., $D^0 \to \rho^0 \mu^+ e^-$) is one in which the number of leptons in each family, electron, muon, or tau, is not conserved in the decay process; i.e. the number of leptons in each family is not conserved between the initial and final states of the decay. The leptons of dissimilar flavors could be created if a horizontal gauge boson existed [11]. With the observation of neutrino oscillations [12], it is now known that lepton flavor conservation is violated at some level.

A LNV decay (e.g., $D^0 \to \pi^- \pi^- \mu^+ \mu^+$) occurs when the number of initial state and final state leptons are not the same. In this analysis a LNV decay is signaled by the presence of two leptons with the same charge, either electrons or muons, in the final state. These decays might involve postulated leptoquarks [13] or Majorana neutrinos [14].

Decays that mimic FCNC decays do exist and can occur at one loop level via box or penguin diagrams via the exchange of charged Ws. They are heavily suppressed by the Glashow-Iliopoulos-Maiani mechanism [15]

and by the small masses of the quark in the loop. The GIM mechanism predicted the existence of the charm quark in order to explain $K_L^0 \rightarrow \mu^+\mu^-$ decays which were observed with much lower rates than predicted by the SM at that time. It was shown that certain decays were suppressed by the interactions involving the charm quarks, which cancelled out the known mode. These short distance diagrams have branching fractions on the order of 10^{-9} [16, 17]. There are also long distance effects whose contributions can be six orders of magnitude greater than the diagrams described above [7, 17]. They involve photon pole amplitudes (see Figure 2.1) and vector meson dominance (VMD). The former is caused by a virtual photon radiating away during a W-exchange decay. The photon decays into the two leptons, while the W-exchange would create the vector meson. The VMD model proceeds via a W decay and the formation of a vector meson that decays via a virtual photon into the $\ell^+\ell^-$ pair. A W radiated by the charm quark could decay into two lighter quarks, one rejoining the now changed charm quark to form the vector meson; the other quark joins the original up quark to form the vector meson that decays into the two leptons. An example of this is $D^0 \rightarrow \bar{K}^{*0}\rho^0$, $\rho^0 \rightarrow e^+e^-$. The branching ratios are $(1.45 \pm 0.32)\%$ and $(4.54 \pm 0.10) \times 10^{-5}$, respectively.

Flavor Changing Neutral Current decay rates that exceed the rates

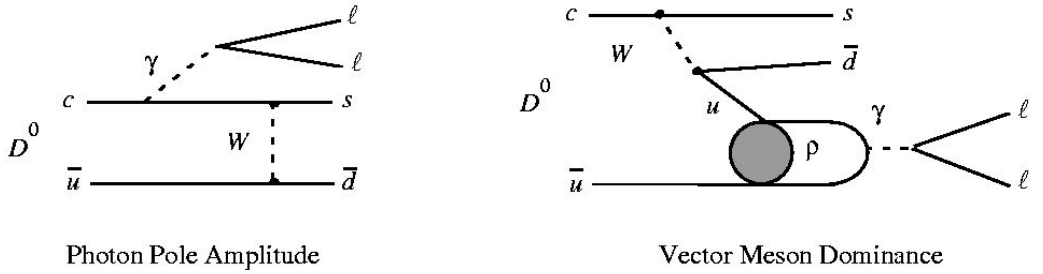

Figure 2.1: Photon Pole Amplitude and Vector Meson Dominance.

expected due to these mechanisms examine physics beyond the Standard Model, while Lepton Flavor Violating decays and Lepton Number Violating decays are unknown within the framework of the Standard Model.

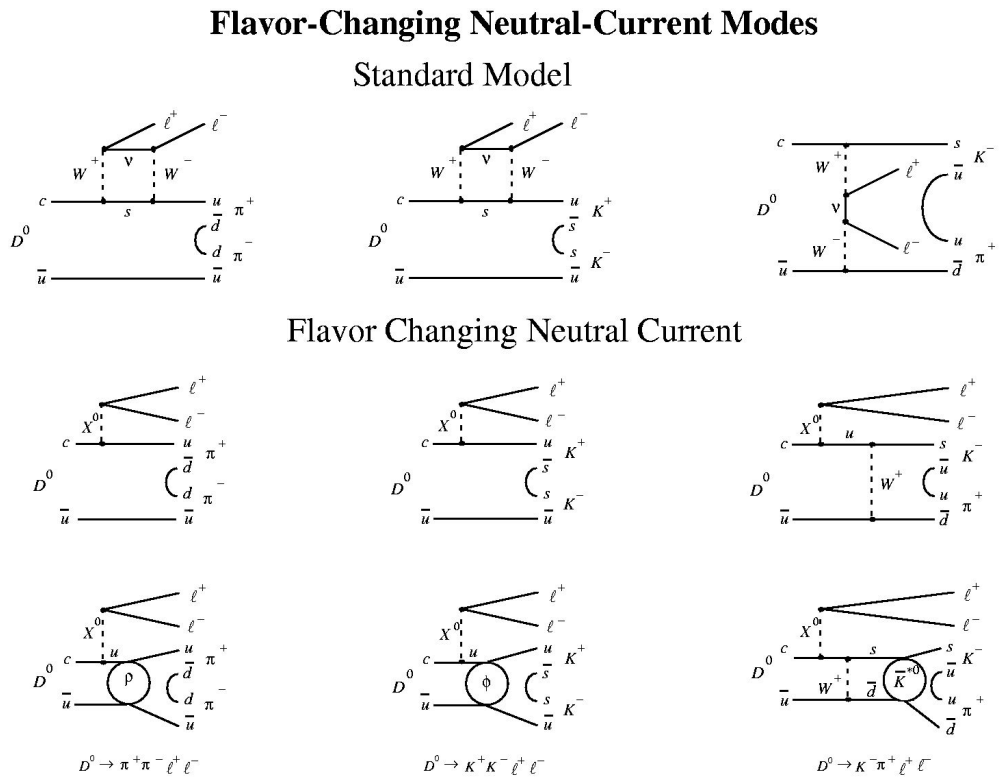

Figure 2.2: Flavor Changing Neutral Current Modes.

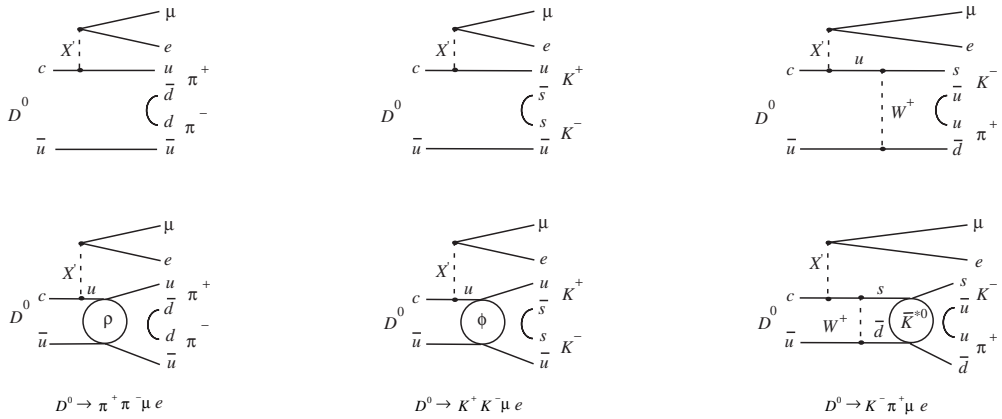

Figure 2.3: Lepton Flavor Violating Modes.

Lepton Number Violating Modes

Lepto-quark

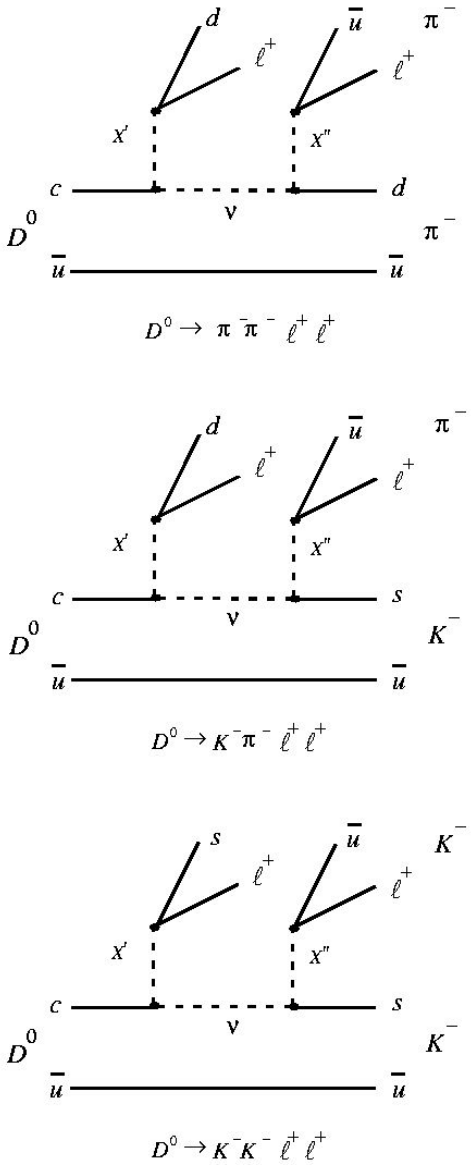

Figure 2.4: Lepton Number Violating Modes.

Chapter 3

The Fermilab Tevatron and the E791 Spectrometer

3.1 The Fermilab Tevatron

The Fermi National Accelerator Laboratory's 800 GeV/c Tevatron accelerated the protons that created the pion beam used in E791. Fermilab is located in Batavia, Illinois. There are five stages to beam acceleration in the Tevatron. First, hydrogen ions (H^-) are produced by passing neutral hydrogen over a cesium source, adding an electron to the atom. The ions are then accelerated by a Cockcroft-Walton accelerator to an energy of 750

keV and injected into the LINAC. Second, the LINAC accelerates the H^- beam to 200 MeV and bunches the beam into buckets with a 19 ns spacing. The ions are then stripped of both electrons and passed to the third stage, an 8 GeV booster ring. The beam intensity is approximately 35-40 mA before booster injection. The booster injects the buckets into the 150 GeV Main Ring. In the final stage, the 150 GeV protons are injected into the Tevatron that accelerates the beam to an energy of 800 GeV. The entire process takes about 34 seconds and results in 2×10^{13} protons orbiting in the Tevatron [18].

The booster and main ring use conventional magnets to bend particle trajectories, while the Tevatron uses higher field superconducting magnets. The beam was extracted to the various experimental areas during a 23 second spill in the switchyard area. The length of this spill increased the time between interactions, giving experiments time to read out data from detectors.

3.2 Beam

The beam used in the E791 experiment at the Tagged Photon Lab consisted of 500 GeV/c negative pions (π^-). These pions were generated from

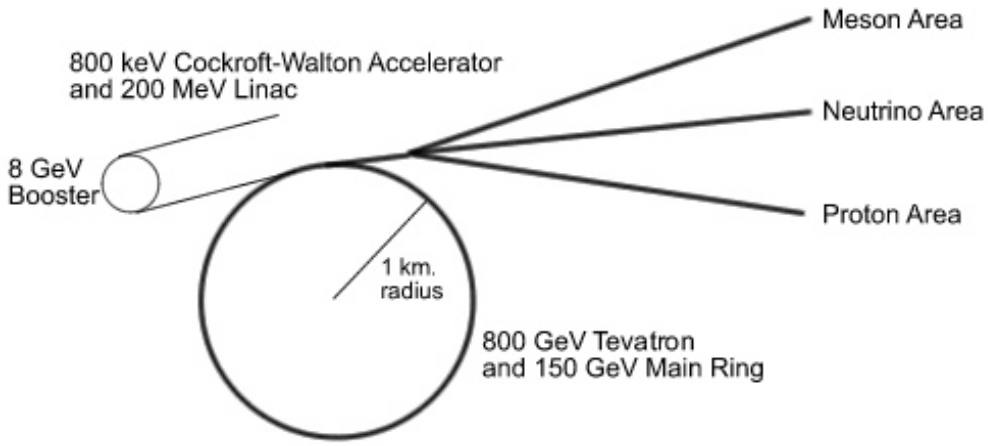

Figure 3.1: Layout of Accelerator and Beamline System.

the interaction of 1.2×10^{12} 800 GeV/c protons/spill with an upstream beryllium target of 30 cm thickness in the Proton Area [19]. The resulting particles were momentum filtered by a dipole magnet and collimated to produce the 500 GeV/c beam of pions. This beam was recollimated and focused by quadrupole and dipole magnets before striking the experiment target to produce interactions including charm quarks. The beam rate for the experiment was 2 million pions per second [3].

3.3 The Tagged Photon Lab Spectrometer

The spectrometer at TPL has been used for many years in the study of charm physics. Previous experiments E516 [20] and E691 [21] used pho-

tons to produce charm, while E769 [22] used hadrons. The spectrometer has undergone several upgrades over the years, but the primary layout has remained constant.

In addition to searching for rare and forbidden charm decays the E791 collaboration has also searched for D^0–$\overline{D}{}^0$ mixing [23], CP violation in D meson decays [24], and pentaquarks [25]. E791 has measured the production characteristics of charmed hadrons [26, 1], observed a doubly Cabibbo–suppressed decay, $D^+ \rightarrow K^+\pi^-\pi^+$ [27], and found evidence for scalar mesons in D decays [28].

The E791 spectrometer used a fixed target and had multiple detectors, including Silicon Microstrip Detector (SMD) planes, drift chambers, Proportional Wire Chamber (PWC) planes, Cerenkov counters, electromagnetic and hadronic calorimeters, and muon identification walls. Major changes were made to the spectrometer after the E769 data run to improve tracking efficiency, muon ID, and to increase the data acquisition rate. A schematic of the spectrometer is shown in Figure 3.2.

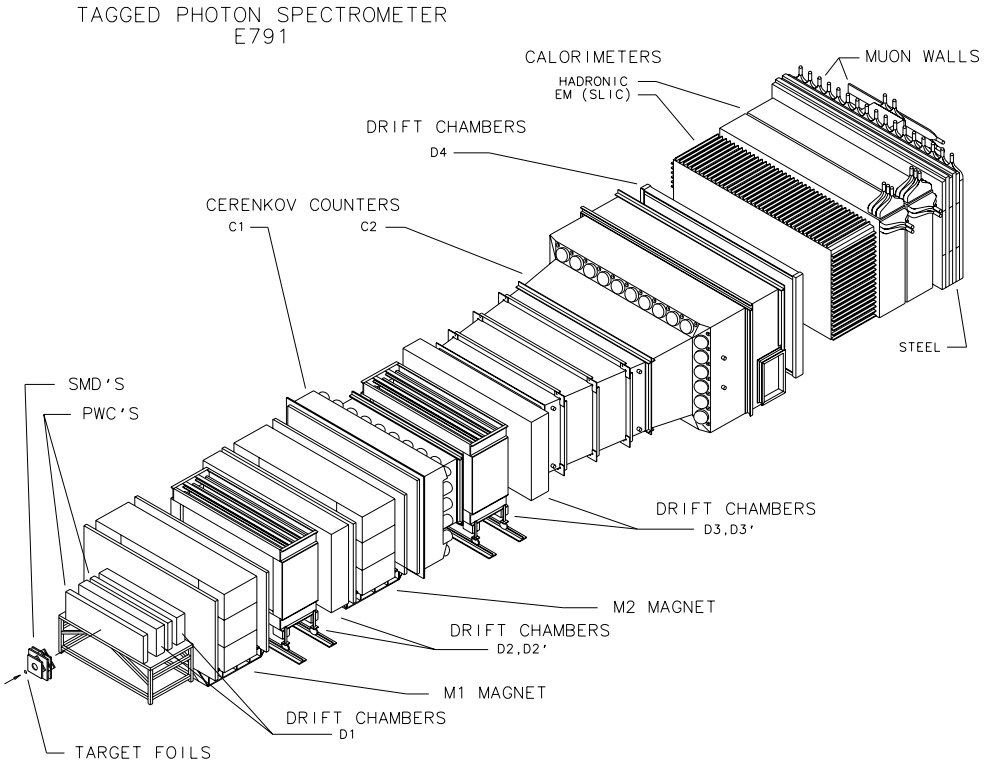

Figure 3.2: The Fermilab E791 Magnetic Spectrometer.

3.4 Beamline PWC and SMD

Before striking the experimental target, the beam passed through a series of Proportional Wire counters (PWC) and Silicon Microstrip Detectors (SMD) to track the beam position. This tracking was vital to the determination of the position of the primary interaction vertex inside the experimental target in the transverse X and Y directions. Z is in the beam direction. There were a total of eight planes of PWCs and six planes of SMDs, an upgrade of four SMD planes from the previous experiment at TPL, E769.

3.5 Experimental Target

The E791 target consisted of five target foils arranged coaxially in a Plexiglas holder that held the foils at a precise separation. The foils were of two different elements, one platinum foil and four carbon (diamond) foils, and were of different thicknesses, 0.5 mm for the Pt target and 1.6 mm for the C targets. The beam pions interacted with the target foils to produce the charm particles. The thinness of the targets allowed a better measurement of the primary vertex Z position while the separation between

Table 3.1: E791 Target Information.

Target Number	1	2	3	4	5
Target Type	Platinum	Diamond	Diamond	Diamond	Diamond
Atomic No.	78	6	6	6	6
Atomic Wt.	195.08	12.01	12.01	12.01	12.01
Thickness (cm)	0.052	0.1572	0.1567	0.1530	0.1544
Diameter (cm)	1.606	1.369	1.377	1.368	1.355
Proton Interaction Lengths	0.00584	0.00590	0.00585	0.00582	0.00587

the targets created sufficient volume to cleanly reconstruct the secondary vertices. The targets allowed 0.4% of the incident pions to interact in each target. An important consideration was the choice of target material which allowed a measurement of the relation between the charm cross section and the atomic number of the target. Therefore, materials with widely different atomic numbers were selected, 195 and 12, respectively.

The carbon targets were synthetic diamonds normally used for oil well drill bits and were purchased from General Electric Superabrasives. The diamonds include about 6% air by volume and may contain up to .5% Cobalt. The platinum was 99.95% pure and certified by the government of Australia.

3.6 Trigger

The E791 experiment used a very loose trigger, allowing the spectrometer to record a large quantity of charm. A loose transverse energy (ET) cut, as measured by the electromagnetic and hadronic calorimeters, was applied to increase the likelihood of detecting charmed particles. The decay of charmed particles creates events in which the decay products have a larger amount of transverse energy and momentum than in light quark particle decays. Events were rejected if two beam particles were in coincidence, as these might fake a high transverse energy event [3].

3.7 Downstream SMD

The Silicon Microstrip Detector (SMD) plane system was of primary importance in the tracking of the decay particle tracks. The typical charm particle traveled 5 to 10 mm in the E791 spectrometer before decaying. The SMD system tracked the flight of these decay products close to the target and achieved a high resolution due to the narrowness of the SMD strips. Nine SMD planes were first used in E691 [29].

Also, the high efficiency of the SMD system greatly enhanced the particle

tracking of the spectrometer. To increase the tracking and reconstruction efficiency six new planes were added for E791, bringing the total number of downstream planes to seventeen. There were three different orientations of SMD planes, X, Y, and V, where the V planes were rotated 20.5 degrees with respect to the vertical X-axis.

An SMD plane consisted of a 300 micron thick sandwich of aluminum strips, arsenic and boron doped silicon, and an aluminum base that creates a reverse p-i-n type diode. When a charged particle passes through the SMD plane it produces approximately 25,000 electron/positron hole pairs in the electron deficient silicon region [19].

The electron holes drift towards the p-type boron and are collected by the surface aluminum strips due the potential difference across the plane. The aluminum strips on the surface are kept at 70 to 90 volts potential difference with respect to the Al base depending on the plane. There were two different plane configurations, one with 25 micron spacing from the center of each strip and the other with 50 micron spacing. The two configurations have efficiencies of 70% and 92% respectively, the 25 micron planes being less efficient due to electronic noise limitations.

The SMDs have been used by the E791 experiment to measure the

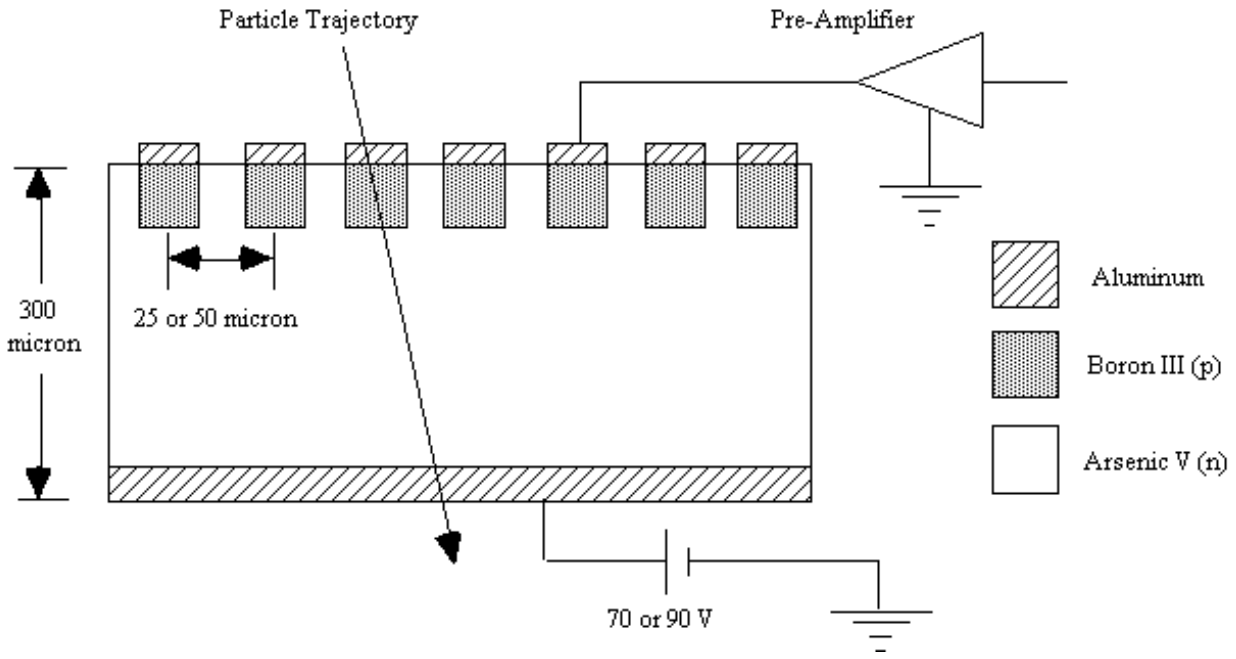

Figure 3.3: Silicon Microstrip Detector (SMD) Schematic.

lifetimes of charmed hadrons such as the D_S^+ [30].

3.8 Downstream PWC

Additionally, two downstream planes of Proportional Wire counters (PWC) were used to increase the Y-direction track resolution and for tracking redundancy. The PWCs collect electrons produced when a charged particle ionizes the chamber gas. The gas used in the PWC was a mixture of 83% Ar, 17% CO2, and 0.3% Freon. The spacing between the wires was 2

mm, producing a resolution of 600 microns.

3.9 Drift Chambers

The drift chamber (DC) system [18, 19] at TPL was used to track the flight of the decay products of the charmed particles as they moved through the spectrometer. Thirty-five planes of sense wires were distributed through seven separate gas boxes and four DC modules. The first module (D1) was located in front of the first analysis magnet (M1), the second module (D2) was located between M1 and the second analysis magnet (M2), the third module (D3) was located after M2, and the fourth module was located after the second Cerenkov counter (C2). In each chamber the assemblies contained different numbers of sense wire planes, four in D1 and three in D2, D3, and D4. The number of sense wires in each plane varied from 96 to 256. (See Table 3.2 for DC specifications.) The orientations of the sense planes were in the X, U, and V directions, where the U and V sense planes are at an angle of $\pm 20.5^0$ with respect to the vertical X-axis. (See Figure 3.4.)

Also, two X planes in D1 were offset a half cell width to define a new plane labeled X'. The X' planes aided in resolving left-right ambiguities in

Table 3.2: Drift Chamber Specifications

Chamber	D1	D2	D3	D4
Assemblies	2	4	4	1
Planes/Assembly	4	3	3	3
Plane Order	UVXX'	UVX	UVX	UVX
Assembly Area	0.91 m^2	3.9 m^2	4.6 m^2	13.3 m^2
Horizontal source wire separation	0.47625 cm	0.9525 cm	1.5875 cm	3.175 cm

track finding and aid in track separation. These planes were located in the center section of D1 because of the high particle flux in that area. A drift chamber plane consisted of three planes of wires, two planes of high voltage cathode wires and one plane of sense wires and field shaping wires. The sense wires were 25 micron gold plated tungsten while the HV wires were 125 micron Be-Cu. The HV planes were held at about -2.4 kV while the field shaping wires were at about -2.0 kV. The sense wires at ground. Adjacent planes of sense wires in the same assembly shared the HV plane between them.

When a charged particle passed through a drift chamber it ionized the gas in the chamber. In E791 the gas used was a non-flammable mixture of 89% argon, 10% carbon dioxide, and 1% CF4 [3]. The electrons produced

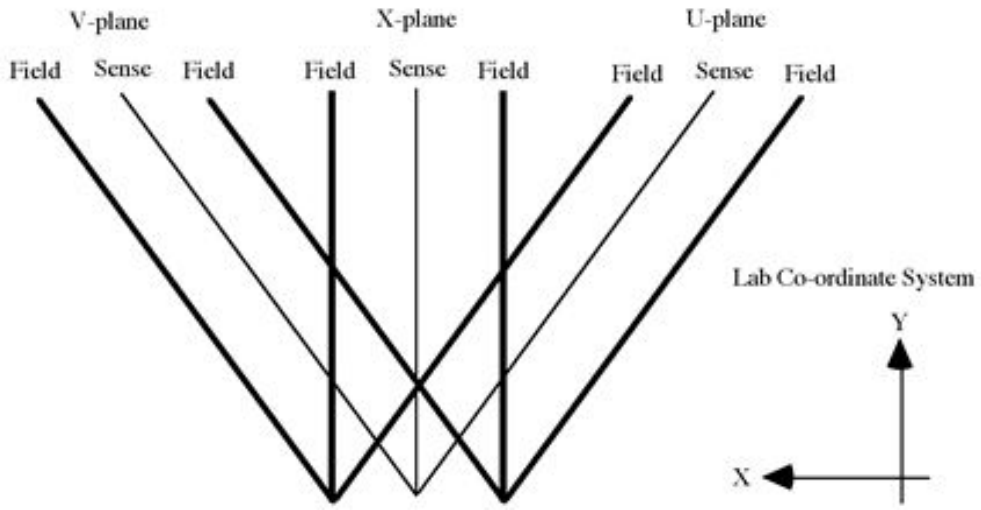

Figure 3.4: Drift Chamber Wire Plane Orientation.

are then amplified and collected by the sense wires due to the field produced by the negative HV and field planes. The signal collected is then further amplified and passed through a discriminator, allowing adjustments of the signal to noise ratio.

3.10 Magnets

The two analysis magnets, M1 and M2, were located between D1 and D2, and D2 and the first Cerenkov detector (C1), respectively. The magnetic field in each magnet was oriented in the vertical direction. The magnets gave incoming charged particles a transverse momentum (p_t) kick according

to the Lorentz force law. This transverse kick, when combined with the drift chamber tracking, provided information about the particle's momentum and charge. The magnets were operated at 2500 (M1) and 1800 (M2) Amps and provided p_t kicks of -212.4 MeV/c and -320.7 MeV/c [18].

3.11 Cerenkov Counters

The threshold Cerenkov detectors [31, 18, 19] were used for particle identification; collecting the light produced by particles moving above the speed of light in the counter gas. The detector gases were chosen to provide identification over the wide range of possible particle momenta. The upstream detector (C1) was filled with pure nitrogen, while the downstream detector (C2) was filled with an 80% helium and 20% nitrogen mixture, and both detectors were held at atmospheric pressure. The phototube faces in C2 were flushed with nitrogen to prevent helium from penetrating the PMT window and damaging the tube. The threshold counter momenta are given in Table 3.3.

The gas mixture in C2 was measured using a Sonic Wave Monitor (SWM) system and monitored using the Low Voltage Monitoring (LVMON) system. The SWM measured the speed of sound in a cylinder filled with

Table 3.3: Cerenkov Counter Particle Momentum Thresholds.

Particle Type	C1 Momentum Threshold (GeV/c)	C2 Momentum Threshold (GeV/c)
π	5.4	10.5
K	18.7	37.2
p	35.5	70.7
e	0.019	0.038
μ	4.01	7.99

gas pumped in from the C2 detector [32]. This speed was converted to a DC voltage and was calibrated via a reference source of 80/20 He/N_2 to determine the nominal output voltage. The LVMON system then read out the voltage and recorded it for future reference. The C2 gas mixture was also monitored periodically using a mass spectrometer.

The LVMON subsystem was responsible for monitoring all the low voltage power systems in E791. There were 192 channels of readouts ranging from the SMD, C1 and C2, DC, to the Exabyte tape drive power supplies. Each channel was read out through an analog-to-digital converter (ADC), with a possible range of 0 to 10 Volts or -5 to +5 Volts. Six ADC modules were used. The ADCs were then latched in the middle of the beam spill, since some detector power supplies would vary depending on the presence

of beam, and readout via the CAMAC crate system [33]. The CAMAC readout was controlled by the LVMON computer program that compared the readout voltage to the voltage standards file. If the detector voltage was outside of a preset limit, the program would display a warning message in the TPL control room. The voltages would then be written approximately once per hour to a disk file on the TPL VAX 11/780.

There were 32 Photomultiplier Tubes (PMT) in C1 and 28 in C2. The incoming photons in each detector were reflected by mirror planes into Winston light collecting cones in front of each PMT face. In C1 two planes of mirrors were used to reflect the incoming light to compress the chamber and allow it to fit in and between the M2 magnet and the D3 drift chamber, just downstream of M2. Also, light baffles were installed in C1 to block Cerenkov radiation produced by beam particles passing through the detector and e^+e^- pairs in a plane at beam height.

The proximity of C1 to the M1 analysis magnet produced minor problems. The central field produced by M1 was on the order of 10,000 Gauss, and produced a small, but not negligible fringe field, in the vicinity of the PMTs [31]. The field affected the efficiency of the tubes by affecting the path taken by the electrons cascading from the dynodes to the anode and reducing the number of electrons that reached the anode [34]. To elim-

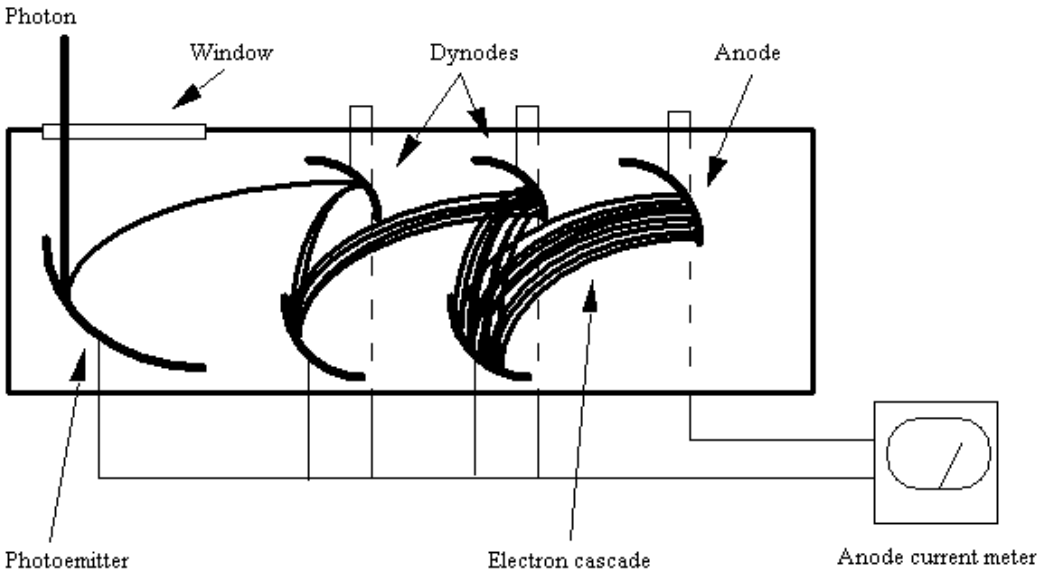

Figure 3.5: Photomultiplier Tube Schematic. The phototubes at TPL worked in a similar fashion to this PMT but had front, rather than side, windows.

inate this effect the tubes were shielded with iron and mu-metal shields. This was determined to be insufficient; therefore each tube was wrapped in a bucking coil. These coils produced an opposing magnetic field when a current of sufficient magnitude was supplied. However, determining the correct current to be supplied proved to be difficult. Various methods were tried to determine the correct current by examining the tube efficiency, the single photo-electron peak (SPEP), and using a laser to measure the tube response. Finally, the brute force method was used; measuring the magnetic field at the tube face directly with a Hall Probe and adjusting the bucking coil current to reduce the field as much as possible. It was determined that the magnetic fields produced by M1 were on the order of a few to ten gauss,

which is sufficient to alter the PMT response if the bucking coils were not present.

3.12 Segmented Liquid Ionization Calorimeter (SLIC)

The Segmented Liquid Ionization Calorimeter (SLIC) was used to measure the energy of the decay particles produced in the experiment such as electrons and photons [35]. The SLIC was designed to detect particles that primarily interact through electromagnetic processes, although some hadronic reactions were also detected. Electrons from semileptonic decays of D mesons have been used by E791 to measure form factors [36].

The SLIC consisted of 60 layers in the beam direction and was oriented in three directions, U, V, and Y, using the standard convention. Each layer is composed of a radiator-scintillator pair. The radiator was a 0.37 cm thick laminate of Al-Pb-Al and each laminate covered the entire area of the detector. The scintillators were square corrugated, aluminum sheets forming the U, V, and Y channels of the SLIC. The channels were lined with teflon and filled with a liquid scintillator, NE235A - teflon having a lower

index of refraction than the scintillator. The light produced was reflected down the channel, due to total internal reflection, and was collected in PMTs using wavebars with wavelength shifters.

3.13 Hadrometer

The Hadrometer [37] was designed to detect hadronic processes only, and was important for the detection of neutral hadrons, such as the neutron and K_L^0. Both the Hadrometer and the SLIC were used in the experiment's ET trigger.

The Hadrometer was constructed of 36 radiator-scintillator assemblies, the first and last 18 assemblies grouped to form upstream/downstream sections. The radiators were 2.5 cm thick steel plates covering the entire detector area. The scintillators were doped acrylic strips with an attached light guide [38]. Each strip was 14.3 cm wide and 1 cm thick. The Hadrometer sections had alternating planes of vertical and horizontal scintillator strips. In each section, the vertical and horizontal strips with the same X or Y orientation were grouped together by light guides and a common phototube.

3.14 Muon Walls

The SLIC and Hadrometer absorb most of the particles produced in the experiment, with the exception of neutrinos, muons, and a small number of hadrons, such as neutrons. Since leptonic and semi-leptonic decay modes are of interest, information concerning the muons must be collected. To identify the muons, the hadrons which happen to pass through the calorimeters must be filtered out. A meter thick steel wall behind the hadrometer absorbs tails of hadronic showers, while allowing the muons through. Two walls of scintillator paddles, placed behind the steel wall, were used in E791 for the detection of muons. The passage of muons through the paddles created photons that could be detected. The paddles were made of scintillator with attached light guides and photomultiplier tubes. The first plane (5.5 m $\times$ 3.0 m) of 15 counters measured the horizontal position while the second plane (3.0 m $\times$ 2.2 m) of 16 counters measured the vertical position. Timing information from the smaller set of muon scintillation counters was used to improve the horizontal position resolution. The combination of vertical and horizontal walls were used to better associate tracks in the detector to muon hits in the paddles. Counter efficiencies, measured using muons originating from the primary target, were found to be $(99 \pm 1)\%$ for the smaller counters and $(69 \pm 3)\%$ for the larger counters. The addition

in E791 of the second wall of muon scintillator paddles made possible the observation of single muon decays of D mesons. This had not been done with a single wall.

Muons from semileptonic decays of D mesons have been used by E791 to measure form factors [39, 40] and branching ratios [41].

Chapter 4

Data Acquisition System

The data from the experimental detectors were read out by various methods, including latches, analog-to-digital converters (ADC), and to time-to-digital converters (TDC). These readout systems comprised the beginning of the Data Acquisition (DA) system. The digitizers, the number of channels per system, and the fraction of tape each system wrote are recorded in Table 4.1.

The main goal of E791 was to collect a large charm particle sample. To accomplish this a loose trigger system was designed allowing many events to be accepted. The percentage of accepted events, the high beam rate, and a new DA system increased the data sample by a factor of 50 over

the previous experiment, E769 [42]. Therefore, the DA system needed to digitize and record at an extremely high rate due to the large number of events and the large number of data channels, 24 000. All channels in the detector were read out in 50 microseconds, another requirement due to the high beam rate. All the data from the detectors arrived during the 23 second spill were stored, using large Event FIFO Buffers (EFB) [43], and written to tape during the spill and the 34 second interspill period. Without this continuous data writing, the DA system would not have been able to handle the large quantity of data. The data arrived at a rate of 26 Mbytes/sec, but was written to 42 8mm Exabyte tape drives at a rate of 10 Mbytes/sec [44]. The E791 data acquisition team was led by Steve Bracker who got his start in recording data with paper tape at the Cerro Tololo Observatory [45].

The data from each individual event passed along eight separate RS485 32-bit wide data paths. Each detector passed data through a specific data path to an Event FIFO Buffer (EFB) containing 80 Mbytes of DRAM and held that data until the VME crates called for it. The eight Event FIFO Buffers contained a total of 640 Mbytes of DRAM.

There were six VME crates each containing eight Event Buffer Interfaces (EBI), nine VME CPU cards, and two tape drive controllers. (See Figures 4.1 and 4.2.) The VME crates reassembled each event from the eight parts

Table 4.1: Front end digitizers and read out controllers. A word is 32 bits.

System	Drift Chamber	Čerenkov, Calorimeter	Silicon Microvertex	Proportional Wire Chamber	CAMAC
Digitizer	Phillips 10C6 TDC	LeCroy 4300B FERA ADC	Ohio State, Nanometric N339P, Nanometric S710/810 Latches	LeCroy 2731A PCOS Latch	LeCroy 4448 Latch, 4508 PLU, 2551 Scaler
Mean Dead Time	30 μs	30 μs	50 μs	4 μs	30 μs
Pre-Controllers	none	2 LeCroy 4301	81 Princeton Scanners	2 LeCroy 2738	none
Controller	FSCC [46]	DYC [47]	Princeton	DYC	SCC [48]
No. of Controllers	10	2	2	1	1
Channels/System	6304	554	15896	1088	80
EFB Event Size	480 words	160 words	110 words	20 words	11 words
Tape Event Size	300 words	160 words	110 words	20 words	12 words
Tape Fraction	50%	27%	18%	3%	2%

contained in the EFBs. This process was called 'munching' the event. When one VME crate was busy munching an event the next crate in the chain would begin munching its own event. During this process the data were compressed to allow more events to be written to tape. Once this process finished, the data were passed to the 8mm Exabyte tapes drives. Each

of the six VME crates could write events to seven different tape drives at 0.25 Mbytes of data per second each, making an overall write speed of 10 Mbytes/s. In the course of the 1991 run, 20 billion data events were written to tape, using 24 000 8mm tapes with an overall data set of 50 Terabytes [44].

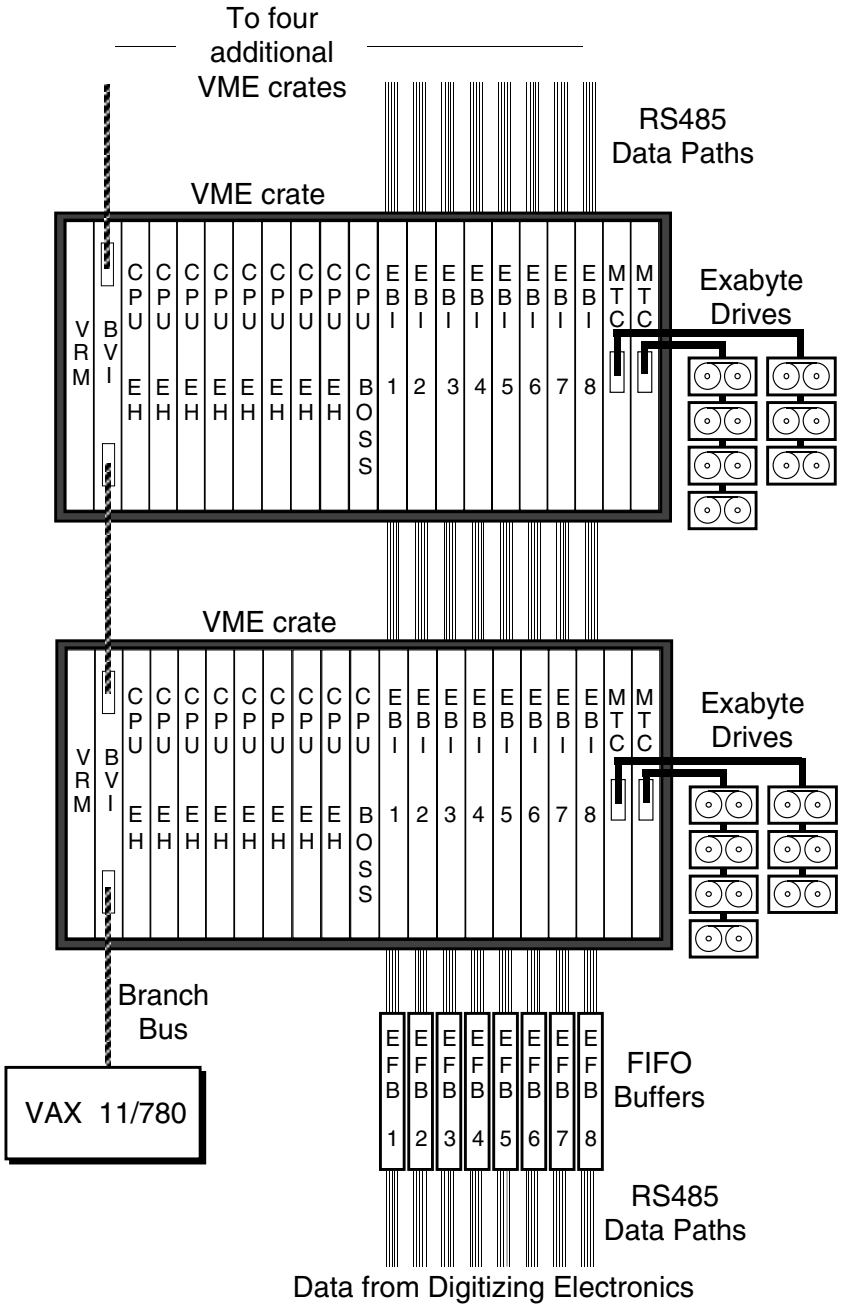

Figure 4.1: A schematic of the VME part of the E–791 DA system [44]. Two complete VME crates are shown, with the Event Fifo Buffers (EFBs) [43] and data paths from the digitizers at the base. Each VME crate was attached to each FIFO to form a 6×8 switching matrix. Six events could thus be built in parallel. Each of the eight FIFOs was attached to two controllers which shared an RS–485 data path.

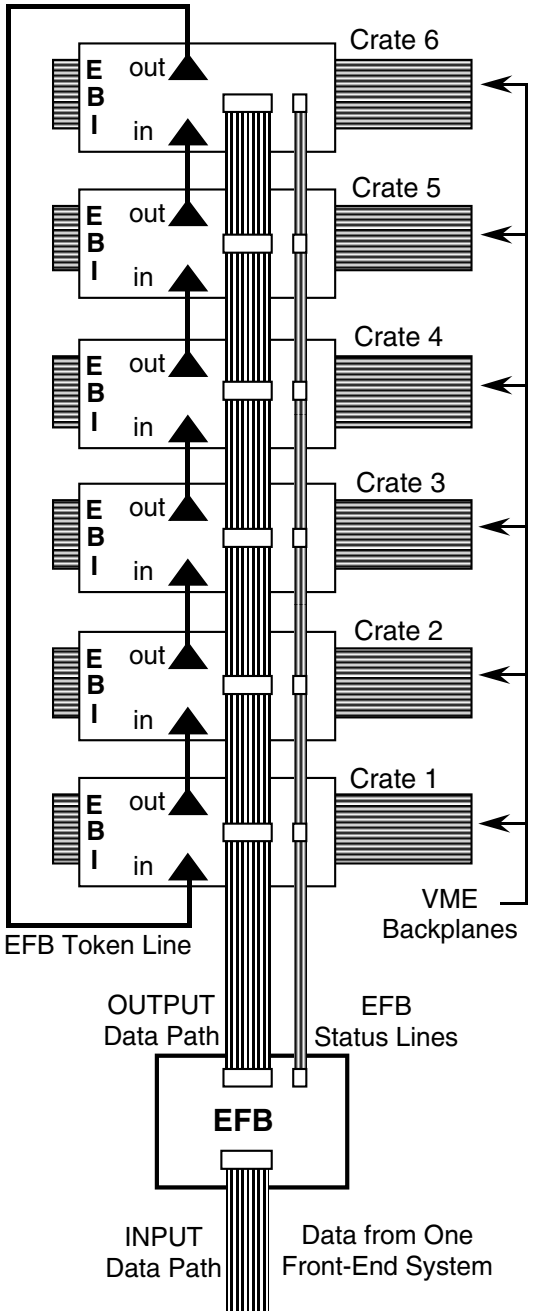

Figure 4.2: Detail of the connections between a single Event FIFO Buffer (EFB) [43] and the six Event Buffer Interfaces (EBIs) attached to it. Each EBI is in a different VME crate. The output data path and the EFB status lines are bussed across all six EBIs. The output data path connects to the VME backplane of each crate through the EBI. The EBIs share the data path by communicating along the EFB token line.

Chapter 5

Data Reconstruction

After the data collecting run at Fermilab was completed, there were 24 000 2–Gigabyte data tapes to be analyzed. To accomplish this daunting task, large computer 'farms' were assembled at the Ohio State University and at the University of Mississippi [49]. Each farm was composed of a large number of independent computers linked through Ethernet and totaling 1000 MIPS (Millions of Instructions Per Second) of computing power. Event processing began in February 1991. Additional farms were then constructed at Fermilab [50] and the Centro Brasileiro de Pesquisas Fisicas; the Ohio farm was moved to the Kansas State University; and the Mississippi and Kansas farms underwent substantial upgrades. The Mississippi computers

utilized were Digital Equipment Corporation's DECstation 5000/200 with 25 MHz MIPS R3000 RISC CPUs and the DECstation 5000/50 with 50 MHz MIPS R4000 RISC CPUs running the ULTRIX operating system. The Mississippi farm was divided into four chains each with independent job managers and a series of client computers. We started with 20 computers and eventually upgraded to a farm of 68 computers. The job manager read out blocks of events from the data tape and passed one block to each of the client computers, which then analyzed the events using the E791 analysis package. The client computer then wrote the reconstructed event to a disk file. The disk files were later moved to a Data Summary Tape (DST). After completing one block of data, the client was ready to accept a new block from the job manager. In this manner each farm operates as a loosely coupled parallel processing system.

The reconstruction or filter program analyzed each event by attempting to link hits in the various detectors into particle tracks and extracting 4-vector momentum from those tracks. The program consists of various smaller subroutines, each with a specific task. A large portion of the program was concerned with finding particle tracks in the detector, a track being defined by hits in various detector channels which form a continuous line in three dimensions. There were two main track subroutines, ESTR

(Exhaustive Search Track Reconstruction) and SESTR (Silicon ESTR) performing similar tasks. SESTR examined the tracks in the SMD system. It attempted to form straight line tracks in the SMD planes and then project that track through the rest of the spectrometer. The projected track can either be straight or bent, depending on the co-ordinate involved. In the horizontal X direction, a charged particle track can be bent by the analysis magnets, while it must be straight in the vertical Y direction. SESTR attempted to connect all tracks in the SMD planes to tracks in the drift chambers. Once completed, SESTR used the bending caused by the analysis magnets to determine the particle momentum.

ESTR operated in the same manner, but using only left over DC tracks,

Figure 5.1: Mississippi farm overview. Servers are on the four tables. Clients are on the racks shown and on desktops not shown. One third of E791's 50 Terabyte raw date set was reconstructed in Mississippi.

i.e., tracks not associated with SMD tracks as found by SESTR. Some particles, such as the Λ^0 and K_S^0, will usually decay after passing through the SMD system, producing tracks only in the DC. ESTR finds these tracks and the associated momenta.

Once the co-ordinates, charge, and momentum of each track was determined, the data from the other detectors were examined. One of the more important parts of the analysis was the determination of the parameters concerning the primary and secondary vertices. The VTXSTR subroutine was the primary vertexing package. It determined if two or more SMD tracks formed a vertex and the parameters of that vertex, such as its co-ordinates and positional error. In the Cerenkov counters, hits in the PMTs were associated with tracks passing through and used in particle type identification. The tracks were then projected through the calorimeter to associate tracks with channel hits to measure the particle energy. The muon walls were used to identify tracks as muons. One in six events were then packaged into the DST format and passed back to a job manager to be written to tape, if the event had a feature of interest such as a secondary vertex. The reconstruction of an entire run of raw data tapes, usually 40, produced about 12-14 DST output tapes. These tapes were copied and sent to the various collaborators on the experiment for analysis and stripping.

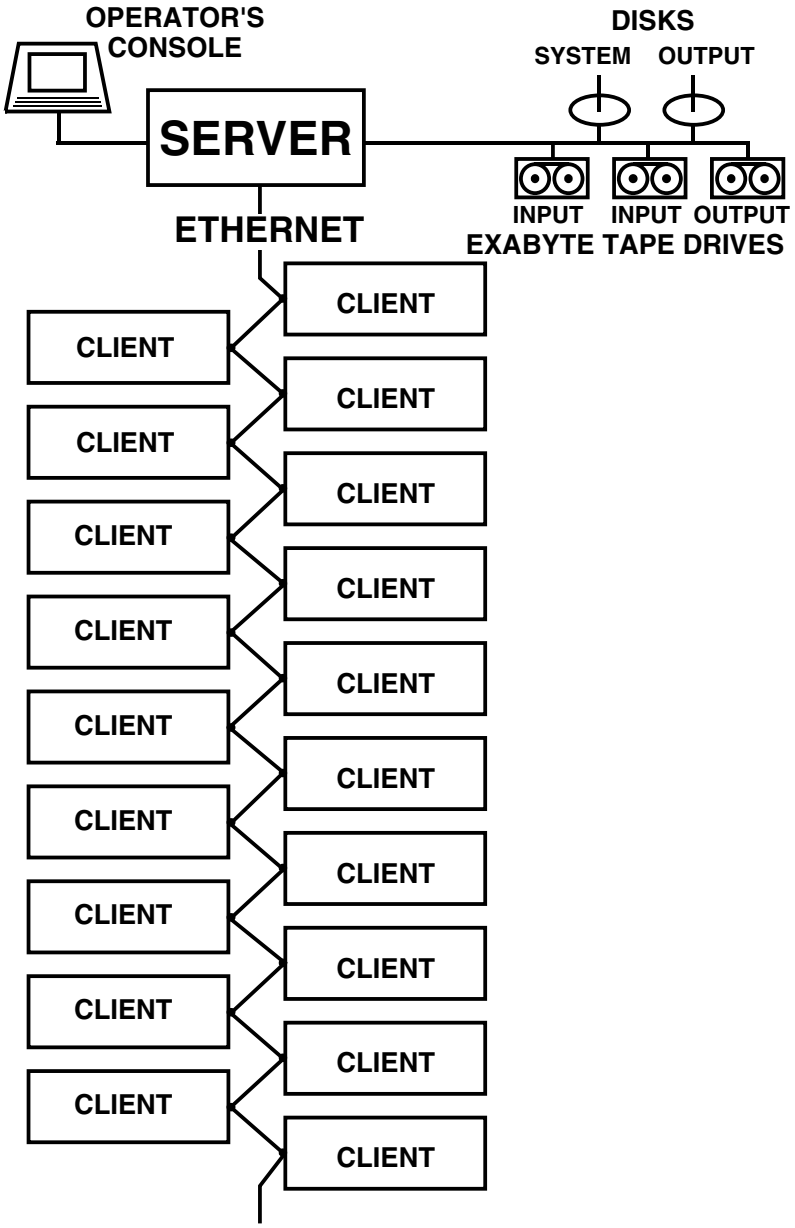

Figure 5.2: Mississippi farm architecture. Servers and clients are DECstation 5000 workstations running ULTRIX. Some have MIPS R3000 CPUs; others the more powerful MIPS R4000. Altogether, there are 68 processors organized into 4 farms isolated by Ethernet bridges. One typical farm is shown here. The two input tape drives alternate automatically. Each drive is only wearing itself out half the time. If an input tape drive fails, the next tape starts automatically. The output is staged through disk and streamed to tape. If the output tape drive fails output data can easily be recovered from disk. If a disk fills, processing is automatically paused until space *appears*. This I/O scheme avoids constant operator supervision.

Chapter 6

Stripping the D meson Signal from the DST Tapes

Once the Data Summary Tapes (DST) are written, the relevant information must be extracted about the particular particle or decay mode of interest via stripping. This involves further analysis of the data on the DST and comes in two basic forms, vertex-list or candidate driven. Each event on the DST contains a list of the all the vertices as calculated by the reconstruction, including the primary. In an event with a charmed hadron, the primary and secondary vertices are separated by several millimeters. In a vertex-list strip, various parameters of each vertex can be calculated and

thus the particles or decays of interest can be stripped out. Additionally, the event can be re-vertexed and any new vertices can be added to the list. A candidate driven strip examines the particles involved in each event and attempts to find the desired decay mode by tracing the particles that give the correct mass to a common vertex. The D meson strip used the vertex-list approach.

The D meson strip was a three part strip, using the multi-stream output (MSO) stripper and two smaller related strips. The MSO stripper examined the DST tapes and could run up to twenty different stripping subroutines simultaneously, writing both to tape and disk files. Various strip subroutines such as a three-prong vertex, $pK\pi$ and $K\pi\pi$, were installed. Each subroutine was designed by various experimenters and used basic cuts to extract the relevant signal.

We started with previous work from the two and three prong rare decays [5] for the kinematic cuts as well as the muon and electron ID cuts, which produced a sizable set of D^0 data.

6.1 Electron Identification

The electron identification was based on the transverse shower shape plus matching the wire chamber tracks to the shower positions and energies in the electromagnetic calorimeter [35]. The electron ID efficiency varied from 62% below 9 GeV/c to 45% above energies of 20 GeV/c. The probability of misidentifying a pion as an electron was 0.8%, independent of the pion momentum.

6.2 Muon Identification

The muon identification was obtained from two planes of scintillation counters. The first plane (5.5 m x 3.0 m) of 15 counters measured the horizontal position while the second plane (3.0 m x 2.2 m) of 16 counters measured the vertical position. Upstream of the counters there were about 15 interaction lengths of shielding to filter out hadrons. Data from $D^+ \rightarrow \bar{K}^{*0}\mu^+\nu_\mu$ decays [39] were used to choose the selection criteria for muon candidates. Timing information from the smaller set of muon scintillation counters was used to improve the horizontal position resolution. Counter efficiencies, measured using muons originating from the primary target, were

found to be $(99 \pm 1)\%$ for the smaller counters and $(69 \pm 3)\%$ for the larger counters. The probability for misidentifying a pion as a muon decreased with momentum, from about 6% at 8 GeV/c to $(1.3 \pm 0.1)\%$ above energies of 20 GeV/c.

6.3 Vertex Cuts

Events with evidence of well-separated primary and secondary vertices were selected to separate charm candidates from background. Secondary vertices had to be separated from the primary vertex by greater than $12\sigma_L$, where σ_L is the calculated resolution of the measured longitudinal separation. Also, the secondary vertex had to be separated from the closest material in the target foils by greater than $5\sigma_L^{'}$, where $\sigma_L^{'}$ is the uncertainty in this separation. The vector sum of the momenta from secondary vertex tracks was required to pass within 40 μm of the primary vertex in the plane perpendicular to the beam. Finally, the net momentum of the charm candidate transverse to the line connecting the production and decay vertices had to be less than 300 MeV/c. Decay track candidates were required to pass approximately 10 times closer to the secondary vertex than to the primary vertex. These selection criteria and kaon identification requirements

were the same for both the search mode and for its normalization signal.

6.4 Vector Meson Mass Cuts

The mass ranges used for the resonant vector mesons were:

$$|m_{\pi^+\pi^-} - m_{\rho^0}| < 150 \text{ MeV/c}^2, \quad (6.1)$$

$$|m_{K^-\pi^+} - m_{\bar{K}^{*0}}| < 55 \text{ MeV/c}^2, \text{ and} \quad (6.2)$$

$$|m_{K^+K^-} - m_{\phi}| < 10 \text{ MeV/c}^2. \quad (6.3)$$

Events in which the mass falls within these ranges are considered resonant, accepting the possibility that a few of these events might be non–resonant. All events outside the mass ranges are considered non–resonant.

The branching ratios for $\rho^0 \to \pi^+\pi^-$, $\overline{K}^{*0} \to K^-\pi^+$, and $\phi \to K^+K^-$ are 1.00, 0.67, and 0.49, respectively. These vector meson masses are 771.1, 896.1, and 1019.5 MeV/c^2, respectively. The $\overline{K}^{*0} \to K^-\pi^+$ branching ratio comes from isospin conservation and Clebsch–Gordon coefficients.

$$|\overline{K}^{*0}> = |I, I_3> = |1/2, 1/2> = \sqrt{2/3}\,|\pi^+ K^-> - \sqrt{1/3}\,|\pi^0 \overline{K}^0> \quad (6.4)$$

$$|K^{*0}> = |I, I_3> = |1/2, -1/2> = \sqrt{1/3}\,|\pi^0 K^0> - \sqrt{2/3}\,|\pi^- K^+> \quad (6.5)$$

6.5 Blind Analysis Technique

To determine our selection cuts we used a "blind" analysis technique. Before the selection criteria were finalized, all events having masses within a window ΔM_S around the mass of the D^0 were "masked" so that the presence or absence of any potential signal candidates would not bias our choice of selection criteria. All criteria were then chosen by studying events generated by a Monte Carlo (MC) simulation program and background events, outside the signal windows, from real data. The criteria were chosen to maximize the ratio $N_{MC}/\sqrt{N_B}$, where N_{MC} and N_B are the numbers of MC and background events, respectively, after all selection criteria were applied. The data within the signal windows were unmasked only after this optimization. We used asymmetric windows for the decay modes containing electrons to allow for the bremsstrahlung low-energy tail. The signal windows were: $1.83 < M(D^0) < 1.90$ GeV/c^2 for $\mu\mu$ and $1.76 < M(D^0) < 1.90$ GeV/c^2 for ee and μe modes. We normalized the sensitivity of our search to topologically similar hadronic 3-body (resonant) or 4-body (non-resonant) decays. One exception to this is the case of $D^0 \to \rho^0 \ell^+ \ell^-$ where we normalize to non–resonant $D^0 \to \pi^+\pi^-\pi^+\pi^-$ because there is no published branching fraction for $D^0 \to \rho^0\pi^+\pi^-$. Table 6.1 lists the normalization mode used for each signal mode and the fitted number of data events (N_{Norm}).

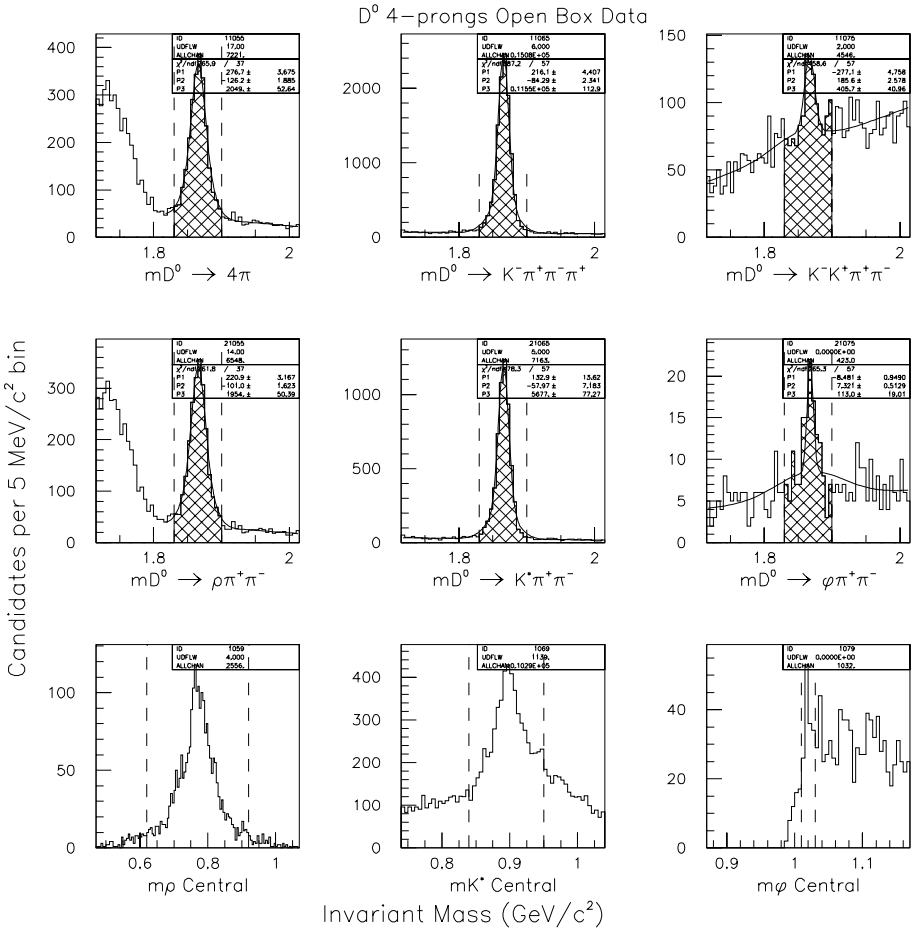

Figure 6.1: Normalization Mode and Vector Meson Decay Plots. Histograms are shown for 2049±53 $D^0 \to \pi^+\pi^-\pi^+\pi^-$ events, 11550±113 $D^0 \to K^-\pi^+\pi^-\pi^+$ events, 406±41 $D^0 \to K^+K^-\pi^+\pi^-$ events, 1954±50 $D^0 \to \rho^0\pi^-\pi^+$, $\rho^0 \to \pi^+\pi^-$ events, 5677±77 $D^0 \to \overline{K}^{*0}\pi^-\pi^+$, $\overline{K}^{*0} \to K^-\pi^+$ events, and 113±19 $D^0 \to \phi\pi^-\pi^+$, $\phi \to K^+K^-$ events. Because it lacks a measured branching ratio, the $D^0 \to \rho^0\pi^-\pi^+$ plot was not used in calculations. The number of $D^0 \to \overline{K}^{*0}\pi^-\pi^+$ events was lowered by 4% for Table 6.1 because of the ambiguity in choosing which π^+ to use to form the $\overline{K}^{*0}$. The vector meson decays $\rho^0(770) \to \pi^+\pi^-$, $\overline{K}^{*0}(892) \to K^-\pi^+$, and $\phi(1020) \to K^+K^-$ are shown in the three plots on the bottom.

Table 6.1: Normalization modes used for $D^0 \to V\ell^+\ell^-$ and $D^0 \to hh\ell\ell$. The $\overline{K}^{*0} \to K^-\pi^+$ and $\phi \to K^+K^-$ branching ratios are included in column 5.

$D^0 \to$	D^0 Norm.	Events	MC Efficiency	Branching Ratio [51]
$\rho^0\ell^\pm\ell^\mp$	$\pi^+\pi^-\pi^+\pi^-$	2049±53	0.95%	$(7.3 \pm 0.5) \times 10^{-3}$
$\overline{K}^{*0}\ell^\pm\ell^\mp$	$\overline{K}^{*0}\pi^+\pi^-$	5451±72	0.28%	$(9.5 \pm 2.1) \times 10^{-3}$
$\phi\ell^\pm\ell^\mp$	$\phi\pi^+\pi^-$	113±19	0.21%	$(5.3 \pm 1.4) \times 10^{-4}$
$\pi\pi\ell\ell$	$\pi^+\pi^-\pi^+\pi^-$	2049±53	0.95%	$(7.3 \pm 0.5) \times 10^{-3}$
$K\pi\ell\ell$	$K^-\pi^+\pi^-\pi^+$	11550±113	0.41%	$(7.49 \pm 0.31)\%$
$KK\ell\ell$	$K^+K^-\pi^+\pi^-$	406±41	0.26%	$(2.5 \pm 0.23) \times 10^{-3}$

The upper limit for each branching fraction B_X is calculated using the following formula:

$$B_X = \frac{N_X}{N_{\rm Norm}} \frac{\varepsilon_{\rm Norm}}{\varepsilon_X} \times B_{\rm Norm};\ \text{where}\ \frac{\varepsilon_{\rm Norm}}{\varepsilon_{\rm X}} = \frac{\rm f_{Norm}^{MC}}{\rm f_X^{MC}}. \tag{6.6}$$

N_X is the 90% confidence level (CL) upper limit on the number of decays for the rare or forbidden decay mode X and B_{Norm} is the normalization mode branching fraction obtained from the Particle Data Group [51]. ϵ_{Norm} and ϵ_X are the detection efficiencies while f_{Norm}^{MC} and f_X^{MC} are the fractions of Monte Carlo events that are reconstructed and pass the final selection

criteria, for the normalization and decay modes, respectively.

6.6 Final D^0 Kinematic Cuts

Here are the final kinematic cuts selected [52]. Initial strips of tapes used somewhat looser cuts. The momentum dependent light yield in the Cerenkov counters was required to be consistent for kaon candidate tracks, except for those in $\phi \rightarrow K^+K^-$ decays, where the narrow ϕ mass window was considered to be sufficient.

- Mass window: 1.715 GeV/c^2 < M(D^0) < 2.015 GeV/c^2
- SDZ > 12
- DZTARG > 5
- TRKXIS < 5
- VITXIS < 6
- XYZVTX < -0.4 cm
- τ < 2.5 ps
- DIP < 0.040 mm

- RATIO < 0.0005
- PTB < 0.300 GeV/c
- "Box":(1.76)1.83 GeV/c^2 $<$ M(D^0) $<$ 1.90 GeV/c^2
- EMPROB > 90 (electrons)

6.7 Cut Variable Definitions

SDZ: The significance of spatial separation from the primary vertex of the secondary vertex, along the beam direction, in standard deviations.

DZTARG: The number of standard deviations the secondary vertex is outside the target.

TRKXIS: The maximum of the fit χ^2 of the reconstructed tracks.

VITXIS: The fit χ^2 of the reconstructed vertex.

XYZVTX: The position along the beam (z-coordinate) direction of the secondary vertex in cm.

Tau: The lifetime (τ) of the parent particle, in picoseconds (ps).

PTB: The component of the parent particle momentum perpendicular to the line joining the primary and secondary vertices, in GeV/c.

DIP: The transverse impact parameter of the parent particle with respect to the primary vertex, in mm.

RATIO: The product, for each reconstructed track in the vertex, of the ratio of the distance between the track and the secondary vertex and of the distance between the track and the primary vertex. Set to $10^{-nprong}$ where nprong is the number of tracks/vertex.

EMPROB: The probability of that track being an electron in percent.

The initial stripping had been previously completed and the events written to tape, so all that remained was to re-strip for events containing a 4-prong secondary vertex, sometimes referred as a SEED3 or SEED4 event. SEED4 vertices contained four tracks while SEED 3 vertices had three tracks with an 'added' nearby fourth track. Once completed, a set of Monte Carlo simulation data was required to set the final cuts enumerated in this chapter.

Chapter 7

Monte Carlo Simulation and Limit Calculations

The TPL spectrometer is a very complex device with many channels of data, planes of detectors, Čerenkov counters, and a complex data acquisition and reconstruction system. The task of measuring the total efficiency would be virtually impossible by any direct physical means. Therefore, the development of computer simulations that are able to numerically model the detector and the particle interactions makes the analysis of HEP data possible. These simulations are called Monte Carlo (MC) programs. They are designed to completely model the detector, the particle interactions,

and simulate the data produced in the experiment using various programs and routines.

7.1 Monte Carlo

The first package is PYTHIA [53]. It is the generator for the MC beam particles and models the interactions between the beam and the target. PYTHIA determines which quarks are created in the primary interaction. Since quarks are not directly observable, they produce 'stable' particles that are seen by the detectors through 'hadronization'. Hadronization is not well understood, but can be modeled by observation of real interactions and some theoretical calculations. Hadronization is handled by the JETSET [53] package that incorporates the LUND fragmentation model. The 'stable' particles are created by JETSET and their properties, such as energy and momentum, are specified. The hadrons produced are then moved through the simulated detectors making hits in various planes, light in the Čerenkov counters, and depositing energy in the calorimeters. The entire spectrometer is simulated using data files which contain information on every aspect of the systems. Position, orientation, interaction lengths, Čerenkov gas, and efficiencies are all included, and many of these data files

are also used by the reconstruction program to perform tracking, for instance. Once the event has been modeled by the MC it is converted to the E791 DST format, with one major addition. The MC adds a 'truth table' to the event record that states exactly what occurred in the event. This truth table is not used in the reconstruction, instead it is examined by a separate program which is used to compare the actual data generated by the MC to the data the reconstruction produces. In this manner the detector efficiencies can be measured.

The process for creating and using an MC tape to measure efficiencies is:

1. The user determines the number, particle type, and decay mode of the events that the MC will generate.

2. The MC program is then run generating a raw MC data tape.

3. The raw MC tape is processed using the reconstruction farm producing an MC DST tape.

4. The DST tape is run through the user's stripping routine and the data of interest is extracted, such as number of hits per target.

5. The raw MC tape is run through a separate program that examines

the 'truth table' for each event. The actual figures for the data of interest are extracted.

6. The results from the stripped DST and the truth tables are compared to measure the total efficiencies.

In this analysis, 250 000 events for each rare decay and normalization mode were created. These events were processed in an identical manner as the raw, real data to generate our set of simulated data. The MC yields are given in Column 7 of Table 7.1, which shows the number of events out of 250 000 that passed the cuts. The efficiencies for the normalization modes (see Table 6.1) varied from approximately 0.2% to 1% depending on the mode.

Monte Carlo studies show that the experiment's acceptances are nearly uniform across the Dalitz plots, except that the dilepton identification efficiencies typically drop to near zero at the dilepton mass threshold. The efficiency typically reaches its full value at masses only a few hundred MeV/c^2 above the dilepton mass threshold. We use a constant weak-decay matrix element when calculating the overall detection efficiencies.

The efficiencies for the search modes varied from approximately 0.05% to 0.34%. We take muon and electron ID efficiencies from data.

7.2 Limit Calculations

The 90% CL upper limits N_X are calculated using the method of Feldman and Cousins [54] to account for background, and then corrected for systematic errors by the method of Cousins and Highland [55]. In these methods, the numbers of signal events are determined by simple counting, not by a fit. All results are shown in Table 7.1 and Figure 7.1. Upper limits are determined using the number of candidate events observed and expected number of background events within the signal region.

Background sources that are not removed by the selection criteria discussed earlier include decays in which hadrons (from real, fully-hadronic decay vertices) are misidentified as leptons. These misidentified leptons can come from hadronic showers reaching muon counters, decays-in-flight, and random overlaps of tracks from otherwise separate decays ("accidental" sources). In the case where kaons are misidentified as pions or leptons, candidate masses shift below signal windows. However, we remove these events to prevent them from influencing our background estimate, which is partially obtained from the mass sidebands (see discussion of N_{Cmb} below). To remove these events prior to the selection-criteria optimization, we reconstruct all candidates as each of the non-resonant normalization modes

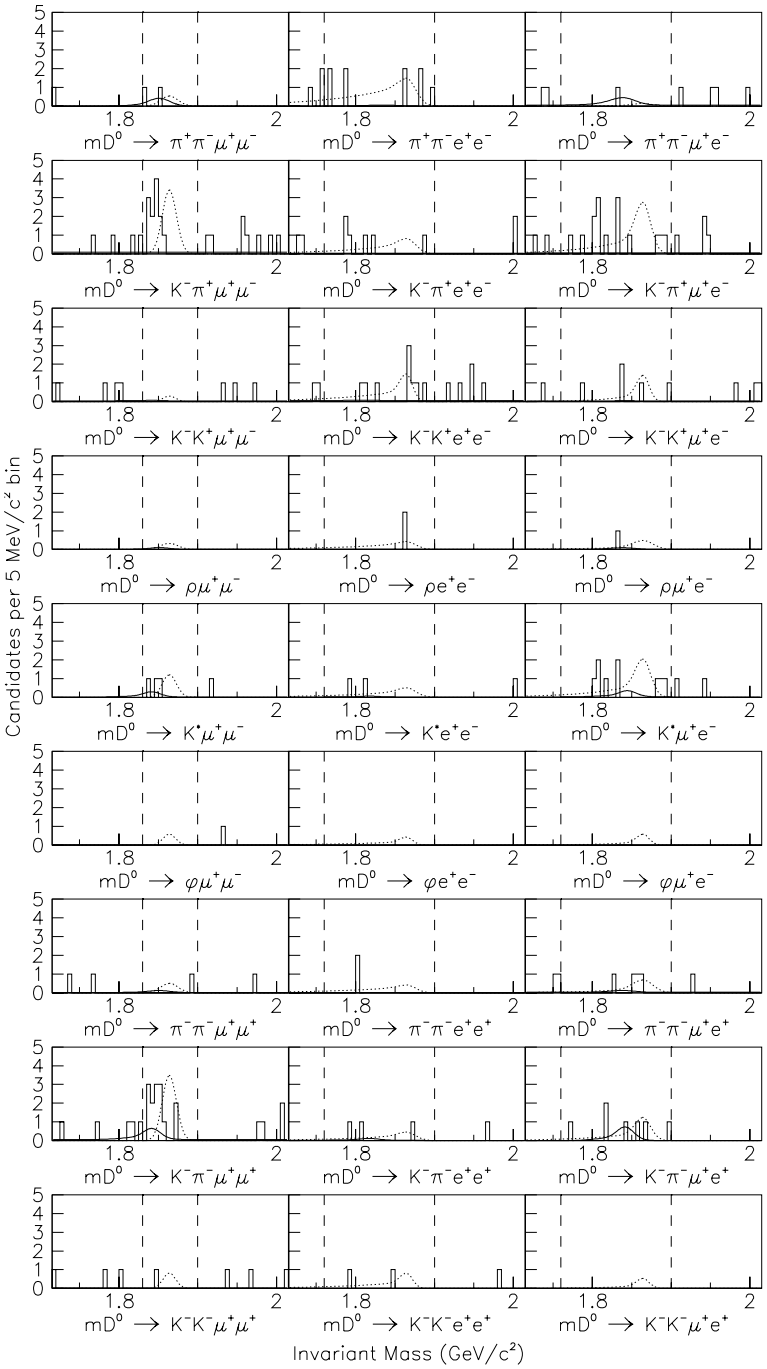

Figure 7.1: Final event samples for the opposite signed dilepton (rows 1–3), resonant (rows 4–6), and same signed dilepton modes (rows 7–9) of D^0 decays. The solid curves display total estimated background; the dotted curves display signal shape for a number of events equal to the 90% CL upper limit. The dashed vertical lines are the ΔM_S boundaries.

Table 7.1: E791 90% confidence level (CL) upper limits on the number of events and branching fraction limits ($\times 10^{-5}$). The Monte Carlo (MC) yield is from 250 000 generated events in each of the 27 cases. Previously published limits are listed for comparison [51, 56, 57].

Mode $D^0 \rightarrow$	(Est. BG) N_{Cmb}	N_{MisID}	N_{Obs}	Sys. Err.	N_X	MC Yield	E791 Limit	PDG Limit
$\pi^+\pi^-\mu^+\mu^-$	0.00	3.16	2	11%	2.96	840	3.0	
$\pi^+\pi^-e^+e^-$	0.00	0.73	9	12%	15.2	345	37.3	
$\pi^+\pi^-\mu^\pm e^\mp$	5.25	3.46	1	15%	1.06	620	1.5	
$K^-\pi^+\mu^+\mu^-$	3.65	0.00	12	11%	15.4	286	35.9	
$K^-\pi^+e^+e^-$	3.50	0.00	6	15%	7.53	135	38.5	
$K^-\pi^+\mu^\pm e^\mp$	5.25	0.00	15	12%	17.3	217	55.3	
$K^+K^-\mu^+\mu^-$	2.13	0.17	0	17%	1.22	145	3.3	
$K^+K^-e^+e^-$	6.13	0.04	9	18%	9.61	120	31.5	
$K^+K^-\mu^\pm e^\mp$	3.50	0.17	5	17%	6.61	149	18	
$\rho^0\mu^+\mu^-$	0.00	0.75	0	10%	1.80	694	2.2	23
$\rho^0e^+e^-$	0.00	0.18	1	12%	4.28	294	12.4	10
$\rho^0\mu^\pm e^\mp$	0.00	0.82	1	11%	3.60	466	6.6	4.9
$\overline{K}^{*0}\mu^+\mu^-$	0.30	1.87	3	24%	5.40	275	2.4	118
$\overline{K}^{*0}e^+e^-$	0.88	0.49	2	25%	4.68	121	4.7	14
$\overline{K}^{*0}\mu^\pm e^\mp$	1.75	2.30	9	24%	12.8	185	8.3	10
$\phi\mu^+\mu^-$	0.30	0.04	0	33%	2.33	187	3.1	41
ϕe^+e^-	0.00	0.01	0	33%	2.75	117	5.9	5.2
$\phi\mu^\pm e^\mp$	0.00	0.05	0	33%	2.71	146	4.7	3.4
$\pi^-\pi^-\mu^+\mu^+$	0.91	0.79	1	9%	2.78	821	2.9	
$\pi^-\pi^-e^+e^+$	0.00	0.18	1	11%	4.26	322	11.2	
$\pi^-\pi^-\mu^+e^+$	2.63	0.86	4	10%	5.18	559	7.9	
$K^-\pi^-\mu^+\mu^+$	2.74	3.96	14	9%	15.7	268	39.0	
$K^-\pi^-e^+e^+$	0.88	1.04	2	16%	4.14	134	20.6	
$K^-\pi^-\mu^+e^+$	0.00	4.88	7	11%	7.81	238	21.8	
$K^-K^-\mu^+\mu^+$	1.22	0.00	1	17%	3.27	137	9.4	
$K^-K^-e^+e^+$	0.88	0.00	2	17%	5.28	137	15.2	
$K^-K^-\mu^+e^+$	0.00	0.00	0	17%	2.52	175	5.7	

and test whether the masses are consistent with m_{D^0}. If so, we remove the events, but only if the number of kaons in the final state differs from that of the search mode. We do not remove events having the same number of kaons, as the loss in acceptance for true signal events would be excessive.

There remain two sources of background: hadronic decays where pions are misidentified as leptons (N_{MisID}) and "combinatoric" background (N_{Cmb}) arising primarily from false vertices and partially reconstructed charm decays. The background (N_{MisID}) arises from the normalization modes. To estimate the rate for misidentifying $\pi\pi$ as $\ell\ell$, for all but the $D^0 \to K^-\pi^+\ell^+\ell^-$ modes, we assume all $D^0 \to K^-\pi^+\ell^+\ell^-$ candidates observed (after subtracting combinatoric background estimated from mass sidebands) result from misidentification of $D^0 \to K^-\pi^+\pi^-\pi^+$ decays and count the number of $D^0 \to K^-\pi^+\ell^+\ell^-$ decays passing the final selection criteria. We then divide by twice the number of $D^0 \to K^-\pi^+\pi^-\pi^+$ normalization events with the $K^-\pi^+\ell^+\ell^-$ mass within ΔM_S boundaries (twice because there are two possible π^+ misidentifications).

From this procedure, the following misidentification rates were obtained: $r_{\mu\mu} = (3.4\pm2.4)\times10^{-4}$, $r_{\mu e} = (4.2\pm1.4)\times10^{-4}$, and $r_{ee} = (9.0\pm6.2)\times10^{-5}$. For modes in which two possible pion combinations can contribute, e.g., $D^0 \to K^-\pi^+\mu^+\mu^-$, we use twice the above rate; and for $D^0\pi^+\pi^-\pi^+\pi^-$

where there are 4 possible combinations, we use 4 times this rate in calculating $D^0 \to \pi^+\pi^-\ell^+\ell^-$. Using these rates, we estimate the numbers of misidentified candidates, $N^{V\ell\ell}_{MisID}$ and $N^{hh\ell\ell}_{MisID}$, in the signal windows as follows:

$$N^{hhll}_{MisID} = r_{\ell\ell} \times N^{hh\pi\pi}_{Norm} \quad \text{and} \quad N^{Vll}_{MisID} = r_{\ell\ell} \times N^{V\pi\pi}_{Norm}, \tag{7.1}$$

where $N^{hh\pi\pi}_{Norm}$ and $N^{V\pi\pi}_{Norm}$ are the numbers of normalization hadronic decay candidates in the signal windows.

To calculate the upper limits for the $D^0 \to K^-\pi^+\ell^+\ell^-$ modes, we set N_{MisID} to zero as we do not have an independent estimate of the misidentification rates. This results in conservative upper limits. If we had used the misidentification rates from our previous, 3-body decay study $K^-\pi^+\ell^+\ell^-$ modes would be lower by about a factor of two.

To estimate the combinatoric background N_{Cmb} within a signal window ΔM_S, we count events having masses within an adjacent background mass window ΔM_B, and scale this number ($N_{\Delta MB}$) by the relative sizes of these windows: $N_{Cmb} = (\Delta M_S/\Delta M_B) \times N_{\Delta MB}$. To be conservative in calculating our 90% confidence level upper limits, we take combinatoric backgrounds to be zero when no events are located above the mass windows. Table 7.1 shows the numbers of combinatoric background, misidentification back-

ground, and observed events for all 27 modes.

The sources of systematic errors [52] in this analysis include: errors from the fit to the normalization sample N_{Norm}; statistical uncertainty on the selection efficiencies, calculated for Monte Carlo simulated events, for both f_{Norm}^{MC} and f_X^{MC}; uncertainties in the calculation of misidentification background; and uncertainties in the relative efficiency for each mode, including lepton tagging efficiencies. These tagging efficiency uncertainties include: 1) muon counter efficiencies from hardware performance; and 2) the fraction of signal events (based on simulations) that $D^0 \to \rho^0 \ell^+ \ell^+$ would remain outside the signal window due to bremsstrahlung tails. Also, for the modes, an additional systematic error is included because we are using $D^0 \to \pi^+\pi^-\pi^+\pi^-$ as the normalization mode since there is no published branching fraction for $D^0 \to \rho^0\pi^+\pi^+$. The sums, taken in quadrature, of these systematic errors are listed in Table 7.1.

7.3 Sample Calculation for $D^0 \to \overline{K}^{*0}\mu^+\mu^-$

A sample calculation for $D^0 \to \overline{K}^{*0}\mu^+\mu^-$ follows:

The number of events observed: $N_{obs} = 3$.

The number of background events: B = .3 (Combinatoric BG) + 1.87 (Mis ID BG) + .26 (Long Range BG) = 2.43.

Systematic Error: $\sigma = .236$ (from [52]).

The long range background comes from the decay of a D^0 to two vector mesons, a $\overline{K}^{*0}$ and a ρ^0. The $\overline{K}^{*0}$ decays to $K^-\pi^+$ and the ρ^0 to $\mu^+\mu^-$.

$$
\begin{aligned}
& N_{LR}(D^0 \to \overline{K}^{*0}\mu^+\mu^-) \qquad (7.2)\\
&= \frac{BF(D^0 \to \overline{K}^{*0}\rho^0) \times BF(\rho^0 \to \mu^+\mu^-)}{BF(D^0 \to \overline{K}^{*0}\pi^+\pi^-)} \times N(D^0 \to \overline{K}^{*0}\pi^+\pi^-)\\
&= \frac{(9.8 \times 10^{-3}) \times (4.6 \times 10^{-5})}{9.5 \times 10^{-3}} \times 5451\\
&= 0.26
\end{aligned}
$$

From Feldman and Cousins [54] 90% confidence level table for three observed events with a background of 2.43 events, we interpolate between backgrounds of 2.0 and 2.5 events, with values of 5.42 and 4.92, respectively. This results in a value for N_{unc}, the number of events uncorrected for the systematic error, of 4.99.

Using Cousins and Highland [55], we can correct for the systematic error via:

$$\Delta N_x = ((N_{unc} + B - N_{obs})/(N_{unc} + B)) \times (N_{unc}^2\,\sigma^2)/2. \qquad (7.3)$$

This results in a value for ΔN_x of .41, which when added to N_{unc} results in a value for N_x of 5.4 events, as shown in Table 7.1.

To calculate the 90% confidence upper limit we utilize Equation 6.6. For this decay we find:

$$N_x = 5.4 \text{ events}, \tag{7.4}$$

$$N_{Norm} = 5451 \text{ events}, \tag{7.5}$$

$$f_{Norm}^{MC} = 694 \text{ normalization MC events out of } 250\,000, \text{ and} \tag{7.6}$$

$$f_X^{MC} = 275 \text{ signal MC events out of } 250\,000. \tag{7.7}$$

For the $D^0 \to \overline{K}^{*0}\pi^+\pi^-$ branching ratio we use the value of $(9.5 \pm 2.1) \times 10^{-3}$ [51], which includes the branching ratio of $\overline{K}^{*0} \to K^-\pi^+$.

$$B_X = \frac{5.4}{5451} \times \frac{694}{275} \times 9.5{\times}10^{-3} = 2.4{\times}10^{-5} \tag{7.8}$$

Chapter 8

Conclusions

In summary, a *blind* analyses has been used to set 90% CL upper limits ranging from 1.5×10^{-5} $(\pi^+\pi^-\mu^\pm e^\mp)$ to 3.9×10^{-4} $(K^-\pi^-\mu^+\mu^+)$ for 27 FCNC and lepton-number/ family violating decays of the D^0. No evidence for any of these 3 and 4-body decays is found [6]. Four limits represent significant improvements over previous results [56, 57]; 18 are new. Figure 8.1 compares the results from E791 with previous experiments, as does Table 7.1.

We have not found flavor changing neutral currents, horizontal gauge bosons, leptoquarks, or Majorana neutrinos.

Work is currently underway at current experiments (e.g. Fermilab FOCUS [58]) and future experiments such as BTeV [59] to further improve the limits presented here or to observe signals.

The Large Hadron Collider at CERN will search for new force media-

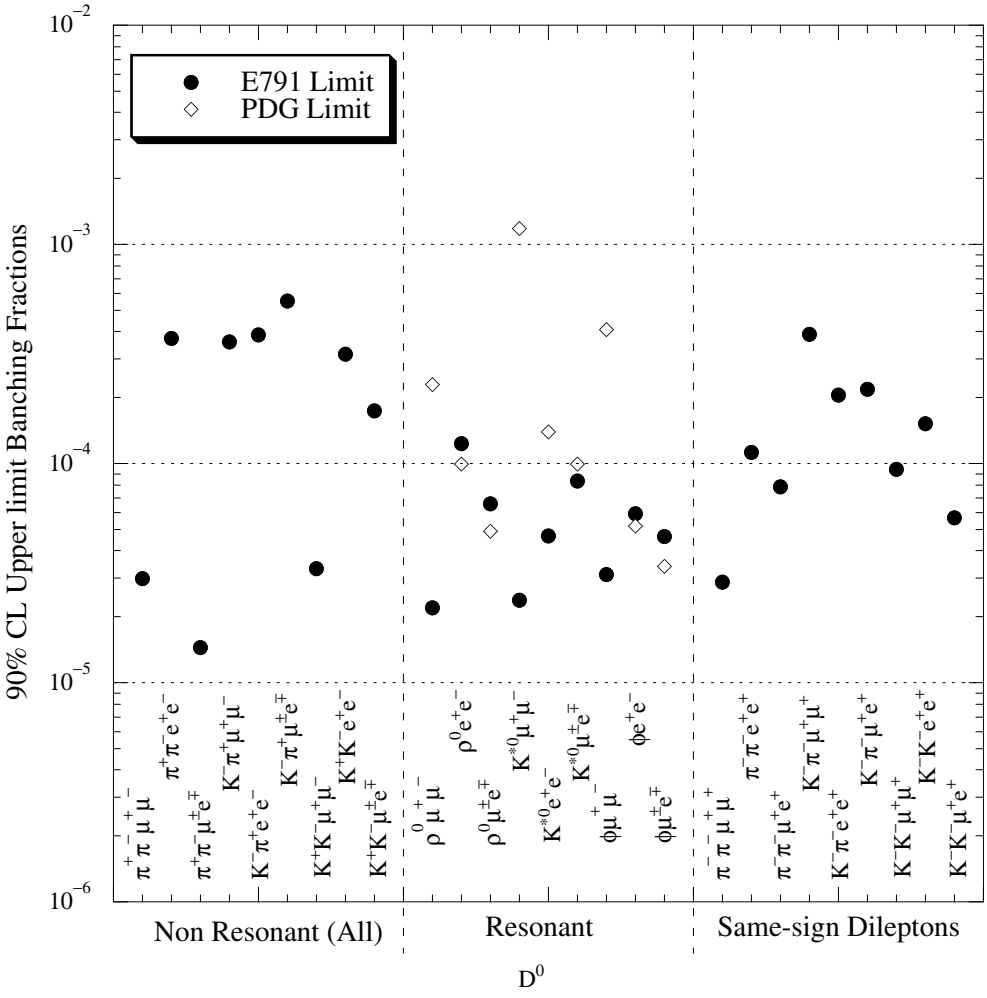

Figure 8.1: Comparison of the 90% CL upper-limit $D^0 \to V\ell^+\ell^-$ and $hh\ell\ell$ branching fractions from E791 data (dark circles) with existing limits (open diamonds) from the 2000 PDG [51].

tors and coupling and may even produce mini black holes [60] that quickly evaporate and branes [61] which are related to string theory. Possible lepton colliders [62] and neutrino factories [63] offer further avenues for discovery.

References

[1] E. M. Aitala *et al.* (E791), *Correlations Between D and $\overline{D}$ Mesons Produced in 500 GeV/c π^--Nucleon Interactions,* EPJdirect **C1** (1999) 4.

[2] L. M. Cremaldi, *Fermilab E791,* ICHEP 92–Dallas, AIP Conf. Proc. **272** (1993) 1058.

[3] D. J. Summers *et al., Charm Physics at Fermilab E791,* XXVII Rencontre de Moriond (15–22 Mar 1992) 417, http://arXiv.org/pdf/hep-ex/0009015.

[4] E. M. Aitala *et al.* (E791), *Search for the Flavor-Changing Neutral Current Decays $D^+ \to \pi^+\mu^+\mu^-$ and $D^+ \to \pi^+e^+e^-$,* Phys. Rev. Lett. **76** (1996) 364;

Nicholas James Witchey (E791), *Search for Flavor Changing Neutral Current Decays of Charm Mesons,* Ph.D. Dissertation, Ohio State University, 1996;

J. Slaughter, *Rare and Forbidden Decays of Charm and Beauty, Mixing in the Charm Sector,* 16^{th} Physics in Collision, Mexico City (19-21 Jun 1996) 189;

A. Nguyen *et al., Recent Results from Fermilab E791,* St. Petersburg 1994, AIP Conf. Proc. **338** (1995) 777.

[5] E. M. Aitala *et al.* (E791), *Search for Rare and Forbidden Dilepton*

Decays of the D^+, D_s^+, and D^0 Charmed Mesons, Phys. Lett. **B462** (1999) 401;

David Sanders, *Search for Rare and Forbidden Dilepton Decays of D^+, D_s^+, and D^0,* E791 Offline Document 393, 77 pages, 1999;

D. A. Sanders, *Recent Results from Fermilab Charm Experiment E791,* DPF 99–Los Angeles (5–9 Jan 1999) http://arXiv.org/pdf/hep-ex/9903067;

D. J. Summers *et al., Search for Rare and Forbidden Charm Meson Decays at Fermilab E791,* XXXV Rencontre de Moriond (11–18 Mar 2000) http://arXiv.org/pdf/hep-ex/0010002.

[6] E. M. Aitala *et al.* (E791), *Search for Rare and Forbidden Charm Meson Decays $D^0 \to V\ell^+\ell^-$ and $hh\ell\ell$*, Phys. Rev. Lett. **86** (2001) 3969;

D. Summers, *Search for Rare 3 and 4-Body D^0 Decays at FNAL E791,* DPF2000–Columbus (9–12 Aug 2000) http://arXiv.org/pdf/hep-ex/0011079;

A. J. Schwartz, *Searches for Rare and Forbidden Decays of Charm: Recent Results from FNAL,* HQ2K–Rio de Janeiro (9-12 Oct 2000) http://arXiv.org/pdf/hep-ex/0101050;

D. A. Sanders *et al., Rare and Forbidden Decays of D mesons,* XXXVI Rencontre de Moriond (10-17 Mar 2001) http://arXiv.org/pdf/hep-

ex/0105028;

D. J. Summers, *Search for Rare Charm Meson Decays at FNAL E791,* FCP 01–Nashville, http://arXiv.org/pdf/hep-ex/0307086.

[7] P. Singer, *Rare Decays of Heavy Quarks: Searching Ground for New Physics,* Acta Phys. Polon. **B30** (1999) 3861;

P. Singer and D.-X. Zhang, *The Long Distance Contribution to* $D \to \pi\ell^+\ell^-$, Phys. Rev. **D55** (1997) 1127.

[8] S. Pakvasa, *Flavor Changing Neutral Currents in Charm Sector (as Signal for New Physics),* FCNC 97–Santa Monica, California, http://arXiv.org/pdf/hep-ph/9705397;

S. Pakvasa, *Charm as Probe of New Physics,* Chin. J. Phys. (Taipei) **32** (1994) 1163;

D. A. Sanders, *Review of Recent Searches for Rare and Forbidden Dilepton Decays of Charmed Mesons,* Mod. Phys. Lett. **A15** (2000) 1399.

[9] G. Burdman and Ian Shipsey, D^0–$\overline{D}{}^0$ *Mixing and Rare Charm Decays,* http://arXiv.org/pdf/hep-ph/0310076;

G. Burdman, E. Golowich, J. Hewett, and S. Pakvasa, *Rare Charm Decays in the Standard Model and Beyond,* Phys. Rev. **D66** (2002) 014009.

[10] G. López Castro, R. Martínez, and J. H. Muñoz, *FCNC in Leptonic and Semileptonic Decays of D mesons in a General Two–Higgs Doublet Model,* Phys. Rev. **D58** (1998) 033003.

[11] J. Chakrabarti, M. Popovic, and R. N. Mohapatra, *Problem of Fermion Generations in Grand Unified Theories,* Phys. Rev. **D21** (1980) 3212;
Hans-Uno Bengtsson, Wei-Shu Hou, A. Soni, and D. H. Stork, *Signatures for Horizontal Gauge Bosons in Very Energetic Hadronic Collisions,* Phys. Rev. Lett. **55** (1985) 2762.

[12] B. T. Cleveland *et al., Measurement of the Solar Electron Neutrino Flux with the Homestake Chlorine Detector,* Astrophys. J. **496** (1998) 505;
Y. Fukuda *et al.* (Super-Kamiokande), *Evidence for Oscillation of Atmospheric Neutrinos,* Phys. Rev. Lett. **81** (1998) 1562;
Q. R. Ahmad *et al.* (SNO), *Direct Evidence for Neutrino Flavor Transformation from Neutral-Current Interactions in the Sudbury Neutrino Observatory,* Phys. Rev. Lett. **89** (2002) 011301;
S. N. Ahmed *et al.* (SNO), *Measurement of the Total Active* ^8B *Solar Neutrino Flux at the Sudbury Neutrino Observatory with Enhanced Neutral Current Sensitivity,* http://arXiv.org/pdf/nucl-ex/0309004;
K. Eguchi *et al.* (KamLAND), *First Results from KamLAND: Evi-*

dence for Reactor Antineutrino Disappearance, Phys. Rev. Lett. **90** (2003) 021802;

M. H. Ahn *et al.* (K2K), *Indications of Neutrino Oscillation in a 250 km Long-Baseline Experiment,* Phys. Rev. Lett. **90** (2003) 041801;

K. Kodama *et al.* (DONUT), *Observation of Tau Neutrino Interactions,* Phys. Lett. **B504** (2001) 218.

[13] J. C. Pati and A. Salem, *Unified Lepton–Hadron Symmetry and a Gauge Theory of the Basic Interactions,* Phys. Rev. **D8** (1973) 1240;

J. C. Pati and A. Salem, *Lepton Number as the Fourth Color,* Phys. Rev. **D10** (1974) 275;

Miriam Leurer, *A Comprehensive Study of Leptoquark Bounds,* Phys. Rev. **D49** (1994) 333;

Miriam Leurer, *Bounds on Vector Leptoquarks,* Phys. Rev. **D50** (1994) 536;

V. M. Abazov *et al.* (D0), *Search for First-Generation Scalar and Vector Leptoquarks,* Phys. Rev. **D64** (2001) 092004;

C. Adloff *et al.* (HERA H1), *A Search for Leptoquark Bosons in e^- p Collisions at HERA,* Phys. Lett. **B523** (2001) 234.

[14] A. Ali, A. V. Borisov, and N. B. Zamorin, *Majorana Neutrinos and Same–Sign Dilepton Production at LHC and in Rare Meson Decays,*

Eur. Phys. J. **C21** (2001) 123.

[15] S. L. Glashow, J. Iliopoulos, and L. Maiani, *Weak Interactions with Lepton-Hadron Symmetry,* Phys. Rev. **D2** (1970) 1285.

[16] A. J. Schwartz, *Overview of Rare and Forbidden Charm Decays,* Mod. Phys. Lett. **A8** (1993) 967.

[17] S. Fajfer, S. Prelovšek, and P. Singer, *Resonant and Nonresonant Contributions to the Weak $D \to V\ell^+\ell^-$ Decays,* Phys. Rev **D58** (1998) 094038;

S. Fajfer, S. Prelovšek, and P. Singer, *Rare Charm Meson Decays $D \to P\ell^+\ell^-$ and $c \to u\ell^+\ell^-$ in the Standard Model and the Minimal Supersymmetric Standard Model,* Phys. Rev **D64** (2001) 114009;

Sasa Prelovšek, *Weak Decays of Heavy Mesons,* Ph.D. Dissertation, Ljubljana University, 2000, http://arXiv.org/pdf/hep-ph/0010106;

Sasa Prelovšek, *Probing New Physics in Rare Charm Processes,* Cairo–2001, http://arXiv.org/pdf/hep-ph/0104159.

[18] Robert Jedicke (E769), *Flavor Dependence of Hadroproduced Charm-Strange Mesons,* Ph.D. Dissertation, University of Toronto, 1992.

[19] Colin W. Gay (E769), *The Charm Cross Section and Atomic Number Dependence in π–N Collisions,* Ph.D. Dissertation, University of

Toronto, 1991.

[20] B. H. Denby *et al.* (E516), *Inelastic and Elastic Photoproduction of J/ψ(3097),* Phys. Rev. Lett. **52** (1984) 795;

G. F. Hartner *et al., A Recoil Proton Detector Using Cylindrical Proportional Chambers and Scintillator Counters,* Nucl. Instrum. Meth. **216** (1983) 113.

[21] J. R. Raab *et al.* (E691), *Measurement of the D^0, D^+, and D_S^+ Lifetimes,* Phs. Rev **D37** (1988) 2391;

R. J. Morrison and M. S. Witherell, *D Mesons,* Ann. Rev. Nucl. Part. Sci. **39** (1989) 183.

[22] G. A. Alves *et al.* (E769), *Feynman–x and Transverse Momentum Dependence of $D^\pm$ and D^0, $\overline{D}{}^0$ Production in 250 GeV π^- – Nucleon Interactions,* Phys. Rev. Lett. **69** (1992) 3147;

G. A. Alves *et al.* (E769), *Atomic Mass Dependence of $D^\pm$ and D^0, $\overline{D}{}^0$ Production in 250 GeV $\pi^\pm$–Nucleon Interactions,* Phys. Rev. Lett. **70** (1992) 722;

G. A. Alves *et al.* (E769), *$D^{*\pm}$ Production in 250 GeV $\pi^\pm N$ Interactions,* Phys. Rev. **D49** (1994) 4317;

G. A. Alves *et al.* (E769), *Enhanced Leading Production of $D^\pm$ and $D^{*\pm}$ in 250 GeV $\pi^\pm$–Nucleon Interactions,* Phys. Rev. Lett. **72** (1994) 812;

G. A. Alves *et al.* (E769), *Forward Cross-sections for Production of* D^+, D^0, D_s, D^{*+}, *and* Λ_C *in 250 GeV* $\pi^{\pm}$, $K^{\pm}$, *and p – Nucleon Interactions,* Phys. Rev. Lett. **77** (1994) 2388;

G. A. Alves *et al.* (E769), *Feynman-x and Transverse Momentum Dependence of D Meson Production in 250 GeV* π, *K, and p – Nucleon Interactions,* Phys. Rev. Lett. **77** (1994) 2392;

G. A. Alves *et al.* (E769), *Atomic Mass Dependence of* Ξ^- *and* $\overline{\Xi}^+$ *Production in Central 250 GeV* π^-*-Nucleon Interactions,* Phys. Rev. **D56** (1997) 6003;

G. A. Alves *et al.* (E769), *Asymmetries in the Production of* Λ^0 *in 250-GeV/c* $\pi^{\pm}$, $K^{\pm}$ *and p–Nucleon Interactions,* Phys. Lett. **B559** (2003) 179.

[23] E. M. Aitala *et al.* (E791), *Search for* D^0–$\overline{D}^0$ *Mixing in Semileptonic Decays,* Phys. Rev. Lett. **77** (1996) 2384;

E. M. Aitala *et al.* (E791), *A Search for* D^0-$\overline{D}^0$ *Mixing and Doubly Cabibbo Suppressed Decays of the* D^0 *in Hadronic Final States,* Phys. Rev. **D57** (1998) 13;

E. M. Aitala *et al.* (E791), *Measurements of Lifetimes and a Limit on the Lifetime Difference in the Neutral D-Meson System,* Phys. Rev. Lett. **83** (1999) 32;

R. Godang *et al.* (CLEO), *Search for D^0–$\overline{D}{}^0$ Mixing,* Phys. Rev. Lett. **84** (2000) 5038;

J. C. Anjos *et al.* (E691), *A Study of D^0–$\overline{D}{}^0$ Mixing,* Phys. Rev. Lett. **60** (1988) 1239;

A. Napier *et al., Results on D^0–$\overline{D}{}^0$ Mixing and Doubly Cabibbo–Suppressed Decays from Fermilab E791,* St. Petersburg, AIP Conf. Proc. **338** (1995) 243;

L. Cremaldi, *Search for Mixing and CP Violation in Charm Decays,* Montreal 1996, Nucl. Phys. Proc. Suppl. **55A** (1997) 221;

M. V. Purohit, *Mixing and CP Violation in the Charm Sector,* HQ 96–St. Goar, Frascati Phys. Ser. **7** (1997) 269.

[24] E. M. Aitala *et al.* (E791), *Search for CP Violation in Charged D Meson Decays,* Phys. Lett. **B403** (1997) 377;

E. M. Aitala *et al.* (E791), *Branching Fractions for $D^0 \to K^+K^-$ and $D^0 \to \pi^+\pi^-$, and a Search for CP Violation in D^0 Decays,* Phys. Lett. **B421** (1998) 405;

J. C. Anjos *et al.* (E691), *Measurement of the Decays $D^0 \to \pi^+\pi^-$ and $D^0 \to K^+K^-$,* Phys. Rev. **D44** (1991) 3371.

[25] E. M. Aitala *et al.* (E791), *Search for the Pentaquark via the $P^0_{\bar{c}s} \to \phi\pi p$ Decay,* Phys. Rev. Lett. **81** (1998) 44;

E. M. Aitala *et al.* (E791), *Search for the Pentaquark via the* $P^{0}_{\bar{c}s} \to K^{*0}K^{-}p$ *Decay,* Phys. Lett. **B448** (1999) 303.

[26] J. A. Appel, *Hadroproduction of Charm Particles,* Ann. Rev. Nucl. Part. Sci. **42** (1992) 367;

E. M. Aitala *et al.* (E791), *Asymmetries between the Production of* D^{+} *and* D^{-} *Mesons from 500 GeV/c* π^{-}*–Nucleus Interactions as a Function of* x_F *and* p_t^2*,* Phys. Lett. **B371** (1996) 157;

E. M. Aitala *et al.* (E791), *Observation of D–*π *Production Correlations in 500 GeV* π^{-}*–N Interactions,* Phys. Lett **B403** (1997) 185;

E. M. Aitala *et al.* (E791), *Asymmetries Between the Production of* $D_{\rm S}^{+}$ *and* $D_{\rm S}^{-}$ *Mesons from 500 GeV/c* π^{-} *Nucleon Interactions as Functions of* x_F *and* p_t^2*,* Phys. Lett. **B411** (1998) 230;

E. M. Aitala *et al.* (E791), *Total Forward and Differential Cross Sections for Neutral–D Mesons Produced in 500 GeV/c* π^{-}*–Nucleon Interactions,* Phys. Lett. **B462** (2000) 225;

E. M. Aitala *et al.* (E791), *Asymmetries in the Production of* Λ_c^{+} *and* Λ_c^{-} *Baryons in 500 GeV/c* π^{-} *Nucleon Interactions,* Phys. Lett. **B495** (2000) 42;

E. M. Aitala *et al.* (E791), *Differential Cross Sections, Charge Production Asymmetry, and Spin Density Matrix Elements for* $D^{*\pm}$(2010)

Produced in 500 GeV/c π^- –Nucleon Interactions, Phys. Lett. **B539** (2002) 218.

[27] E. M. Aitala *et al.* (E791), *The Doubly Cabibbo–Suppressed Decay $D^+ \to K^+\pi^-\pi^+$*, Phys. Lett. **B404** (1997) 187.

[28] E. M. Aitala *et al.* (E791), *Experimental Evidence for a Light and Broad Scalar Resonance in $D^+ \to \pi^+\pi^-\pi^+$ Decay*, Phys. Rev. Lett. **86** (2001) 770;

E. M. Aitala *et al.* (E791), *Study of the $D_s^+ \to \pi^+\pi^-\pi^+$ Decay and Measurement of f_0 Masses and Widths*, Phys. Rev. Lett. **86** (2001) 765;

E. M. Aitala *et al.* (E791), *Dalitz Plot Analysis of the Decay $D^+ \to K^-\pi^+\pi^+$ and Indication of a Low–Mass Scalar $K\pi$ Resonance,* Phys. Rev. Lett. **89** (2002) 121801;

E. M. Aitala *et al.* (E791), *Phase Motion in the Scalar Low-Mass $\pi\pi$ Amplitude in $D^+ \to \pi^-\pi^+\pi^+$ Decay,* Fermilab-Pub-03/296-E.

[29] R. Kumar (E691), *Charm Photoproduction Using a Silicon Vertex Detector,* in *Vertex Detectors,* Plenum Press, Erice (21-26 Sep 1986) 167;

P. Karchin, D. Hale, R. Morrison, M. Witherell, M. Sokoloff, A. Kiang, R. Kumar, J. Martin, and M. Sarabura, *Test Beam Studies of a Silicon Microstrip Vertex Detector,* IEEE Trans. Nucl. Sci. **32** (1985) 612;

P. Karchin *et al., Charm Photoproduction Results from Fermilab E691 and Prospects for Hadroproduction in E769,* Higher Twists, Paris–1988, Nucl. Phys. Proc. Suppl. **7B** (1989) 60.

[30] E. M. Aitala *et al.* (E791), *Measurement of the D_s Lifetime,* Phys. Lett. **B445** (1999) 449;
J. C. Anjos *et al.* (E691), *Measurement of the D_s Lifetime,* Phys. Rev. Lett. **58** (1987) 1818.

[31] D. Bartlett *et al., Performance of the Cerenkov Counters in the Fermilab Tagged Photon Spectrometer Facility,* Nucl. Instrum. Meth. **A260** (1987) 55.

[32] H. Fenker, E769 Internal Memo, *C2 Gas Mixture Monitoring during E769.*

[33] E. Aitala, E791 Internal Document, The LVMON System, 1991.

[34] C. R. Kitchin, *Astrophysical Techniques,* Adam Hilger, Bristol, 1984.

[35] V. K. Bharadwaj *et al., An Inexpensive Large Area Shower Detector with High Spatial and Energy Resolution,* Nucl. Instrum. Meth. **155** (1978) 411;
V. K. Bharadwaj *et al., A Large Area Liquid Scintillation Multi–Photon Detector,* Nucl. Instrum. Meth. **A228** (1985) 283;

D. J. Summers, *Reconstruction of a Strip Geometry Calorimeter Using Stepwise Regression,* Nucl. Instrum. Meth. **A228** (1985) 290.

[36] E. M. Aitala *et al.* (E791), *Measurement of the Form-Factor Ratios for* $D^+ \to \overline{K}^{*0} e^+ \nu_e$*,* Phys. Rev. Lett. **80** (1998) 1393.

[37] J. A. Appel *et al., Hadron Calorimetry at the Fermilab Tagged Photon Spectrometer Facility,* Nucl. Instrum. Meth. **A243** (1986) 361.

[38] J. A. Appel, M. Atac, and P. Mantsch, *High Quality Domestic Acrylic Scintillator and Wave Bar,* (1978) Fermilab-FN-0313.

[39] E. M. Aitala *et al.* (E791), *Measurement of the Form-Factor Ratios for* $D^+ \to \overline{K}^{*0} \ell^+ \nu_\ell$*,* Phys. Lett **B440** (1998) 435.

[40] E. M. Aitala *et al.* (E791), *Measurement of the Form-Factor Ratios for* $D_{\rm s}^+ \to \phi\, \ell^+ \nu_\ell$*,* Phys. Lett. **B450** (1999) 294.

[41] E. M. Aitala *et al.* (E791), *Measurement of the Branching Ratio* $B(D^+ \to \rho^0 \ell^+ \nu_\ell)\ / B(D^+ \to \overline{K}^{*0} \ell^+ \nu_\ell)$*,* Phys. Lett. **B397** (1997) 325.

[42] C. Gay and S. Bracker, *The E769 Multiprocessor Based Data Acquisition System,* IEEE Trans. Nucl. Sci. **34** (1987) 870.

[43] A. E. Baumbaugh *et al., A Real Time Data Compactor (Sparsifier) and 8 Megabyte High Speed FIFO for HEP,* IEEE Trans. Nucl. Sci. **33**

(1986) 903;

K. L. Knickerbocker *et al., High Speed Video Data Acquisition System (VDAS) For HEP, including Reference Frame Subtractor, Data Compactor and 16-Megabyte FIFO,* IEEE Trans. Nucl. Sci. **34** (1987) 245;

A. E. Baumbaugh, K. L. Knickerbocker, B. Baumbaugh, and R. Ruchti, *Operational Experience with a High Speed Video Data Acquisition System in Fermilab Experiment E-687,* IEEE Trans. Nucl. Sci. **35** (1988) 253.

[44] S. Amato, J. R. T. de Mello Neto, J. de Miranda, C. James, D. J. Summers, and S. B. Bracker, *The E791 Parallel Architecture Data Acquisition System,* Nucl. Instrum. Meth. **A324** (1993) 535.

[45] B. M. Lasker, S. B. Bracker, and W. E. Kunkel, *Lunar Occultations from Cerro Tololo I. The Carbon Star, TX Piscium,* Publ. Astron. Soc. Pac. **85** (1973) 109.

[46] D. Berg et al., *Software for the Fermilab Fastbus Smart Crate Controller,* IEEE Trans. Nucl. Sci. **38** (1991) 306.

[47] Steve Bracker and Sten Hansen, *Description of the Damn Yankee Controller (DYC),* http://arXiv.org/pdf/hep-ex/0210034.

[48] S. Hansen, D. Graupman, S. Bracker, and S. Wickert, *Fermilab Smart CAMAC Controller,* IEEE Trans. Nucl. Sci. **34** (1987) 1003;
R. Vignoni *et al., Fermilab Fast Parallel Readout System for Data Acquisition,* IEEE Trans. Nucl. Sci. **34** (1987) 756.

[49] S. Bracker, K. Gounder, K. Hendrix, and D. Summers (E791), *A Simple Multiprocessor Management System for Event–Parallel Computing,* IEEE Trans. Nucl. Sci. **43** (1996) 2457;
D. Summers, S. Bracker, K. Gounder, and K. Hendrix (E791), *An Efficient Multiprocessor Management System for Event–Parallel Computing,* DPF 96–Minneapolis, Minnesota (11–15 August 1996) 1385, http://arXiv.org/pdf/hep-ex/0007003.

[50] C. Stoughton and D. Summers, *Using Multiple RISC CPUs in Parallel to Study Charm Quarks,* Computers in Physics **6** (1992) 371;
F. Rinaldo and S. Wolbers, *Loosely Coupled Parallel Processing at Fermilab,* Computers in Physics **7** (1993) 184.

[51] D. E. Groom *et al.* (Particle Data Group), *Review Of Particle Physics,* Eur. Phys. J. **C15** (2000) 1.

[52] Eric Aitala and David Sanders, *Search for Rare and Forbidden Decays of 4–Particle Decay Modes of D^0,* E791 Offline Document 434, 42

pages, 2001.

[53] T. Sjöstrand, *High–Energy Physics Event Generation with PYTHIA 5.7 and JETSET 7.4,* Comput. Phys. Commun. **82** (1994) 74;

T. Sjöstrand, *Pythia 5.7 and Jetset 7.4: Physics and Manual,* LU-TP-95-20, CERN-TH-7112-93-REV, http://arXiv.org/pdf/hep-ph/9508391.

[54] G. J. Feldman and R. D. Cousins, *A Unified Approach to the Classical Statistical Analysis of Small Signals,* Phys. Rev. **D57** (1998) 3873.

[55] R. D. Cousins and V. L. Highland, *Incorporating Systematic Uncertainties into an Upper Limit,* Nucl. Instrum. Meth. **A320** (1992) 331.

[56] A. Freyberger *et al.* (CLEO), *Limits on Flavor Changing Neutral Currents in D^0 Meson Decays,* Phys. Rev. Lett. **76** (1996) 3065.

[57] K. Kodama *et al.* (E653), *Upper Limits of Charm Hadron Decays to Two Muons Plus Hadrons,* Phys. Lett. **B345** (1995) 85.

[58] J. M. Link *et al.* (E831), *Search for Rare and Forbidden 3 Body Dimuon Decays of the Charmed Mesons D^+ and D_S^+,* Phys. Lett. **B572** (2003) 21;

Paul D. Sheldon, *Charm Mixing and Rare Decays,* Heavy Flavors 8–Southampton (25–29 Jul 1999) http://arXiv.org/pdf/hep-ex/9912016;

Jianwei Cao (E687), *Search for Physics Beyond the Standard Model through Rare and Forbidden Decays of the Charmed D^+ Meson,* Ph. D. Dissertation, Vanderbilt University, 1997.

[59] A. Kulyavtsev *et al., BTeV: An Experiment to Measure Mixing, CP Violation, and Rare Decays of Beauty and Charm at the Fermilab Collider,* ICHEP 2000–Osaka, http://arXiv.org/pdf/hep-ex/0006037.

[60] Marco Cavaglia, *Black Hole Multiplicity at Particle Colliders (Do Black Holes Radiate Mainly on the Brane?),* Phys. Lett. **B569** (2003) 7;

Marco Cavaglia, Saurya Das, and Roy Maartens, *Will We Observe Black Holes at LHC?,* Class. Quant. Grav. **20** (2003) L205.

[61] Eun-Joo Ahn, Marco Cavaglia, and Angela V. Olinto, *Brane Factories,* Phys. Lett. **B551** (2003) 1.

[62] R. B. Palmer, *Prospects for High–Energy e^+ e^- Linear Colliders,* Ann. Rev. Nucl. Part. Sci. **40** (1990) 529;

C. M. Ankenbrandt *et al., Status of Muon Collider Research and Development and Future Plans,* Phys. Rev. ST Accel. Beams **2** (1999) 081001;

R. B. Palmer *et al., Muon Collider Design,* Nucl. Phys. Proc. Suppl.

51A (1996) 61;

Vernon D. Barger, M. S. Berger, J. F. Gunion, and Tao Han, *Higgs Boson Physics in the s–Channel at μ^+ μ^- Colliders,* Phys. Rept. 286 (1997) 1.

[63] C. Albright *et al., Physics at a Neutrino Factory,* 2000, http://arXiv.org/pdf/hep-ph/0008064;

Mohammad M. Alsharo'a *et al., Recent Progress in Neutrino Factory And Muon Collider Research within the Muon Collaboration,* Phys. Rev. ST Accel. Beams **6** (2003) 081001.

[64] Eric Matthew Aitala (E791), *A Study of Atomic Number Dependence of Charm D Meson Hadroproduction,* Master's Thesis, University of Mississippi, 1993.

Vita

The author, Eric Matthew Aitala, was born April 30, 1966 to Mr. and Mrs. Franco Aitala, in upstate New York. Franco Aitala immigrated to the United States from Italy in 1960. Marilyn Aitala (nee Bemis) was born in Hamilton, NY.

He attended Springfield High School in Springfield, Pennsylvania from 1980 to 1984 and graduated in 1984. He then attended the Pennsylvania State University from 1984 to 1988, where he received a Bachelor of Science degree in Astronomy in May, 1988. Eric then studied at the University of Mississippi, in the field of physics with the UM High Energy Physics Group. During the course of his enrollment, he worked with the E791 HEP Collaboration at Fermilab in Batavia, Illinois from 1989 to 1993. He completed a Master of Science thesis [64] in physics at the University of Mississippi in 1993.

Eric also taught and helped develop the undergraduate Astronomy Laboratory and Astronomy Open House at Ole Miss and is one of the Astronomy Lab Manual's authors along with Dr. Donald Summers. Eric also presented various talks to local school children on the subject of Astronomy. His interests include Ultimate Frisbee and foil fencing, having helped establish the fencing clubs at Penn State and Ole Miss.

Eric is currently employed as the University of Mississippi–Oxford Webmaster.